UNIVERSITY OF OKLAHOMA

GRADUATE COLLEGE

Atmospheric Conditions Preceding Very Rapid Sea Ice Loss Events

A THESIS

SUBMITTED TO THE GRADUATE FACULTY

in partial fulfillment of the requirements for the

Degree of

MASTER OF SCIENCE IN METEOROLOGY

By

MADELINE CLARK FRANK
Norman, Oklahoma
2019

Atmospheric Conditions Preceding Very Rapid Sea Ice Loss Events

A THESIS APPROVED FOR THE
SCHOOL OF METEOROLOGY

BY

Dr. Steven Cavallo, Chair

Dr. David Parsons

Dr. Jason C. Furtado

Acknowledgments

I would like to thank all of the Arctic and Antarctic Research Group for their overwhelming support for this project, but especially my advisor, Dr. Cavallo, and Nick Szapiro. I've learned so much in the last two years and can't wait to see what's next. I would also like to thank my husband, Liam, for encouraging me through the weird hours, late nights, and an inability to talk about anything other than sea ice for several months. To all my other family, friends, and colleagues, thank you. I wouldn't be here without you.

Table of Contents

List of Tables

List of Figures

Abstract

Even though the observed amplified warming trend in the Arctic region is well-established in theory through climate feedbacks and reproduced in global climate model projections, the same global climate models underestimate the corresponding decline in Arctic sea ice extent. Even some of the most sophisticated global climate models do not reproduce the observed characteristics or trends in present day Arctic cyclones. These results would indicate that a deeper understanding of the ocean-atmosphere interface is critical to improving both forecasting and analysis of stronger storms – systems that have the potential to both interfere with maritime transport and act to increase sea-ice loss. Periods of significant sea ice loss have been observed in conjunction with extreme cyclones during the summer, such as the "Great Arctic Cyclone" in August 2012. We refer to such sea ice loss events that occur over a few days as very rapid sea ice loss events. The goals of this thesis are two fold: 1.) To establish that a relationship between Tropopause Polar Vortices, surface cyclones, and very rapid sea ice loss events (VRILEs) exists and 2.) To characterize what atmospheric and sea ice conditions are ideal for VRILEs to occur. We hypothesize that long-lived Arctic cyclones located over thin ice have the greatest impact on sea ice loss.

After identifying the time and location of the VRILEs using sea ice extent and concentration data from the National Snow and Ice Data Center, we composite cases separately for summer (JJA) and winter (DJF) events. Results show that on average during the summer, very rapid sea ice loss events occur in a region of particularly strong pressure gradient between an Arctic cyclone and high pressure over the Beaufort Sea. During winter, very rapid sea ice loss events occur when the pressure gradient region of cyclones entering the Arctic from midlatitude storm tracks is strong over the marginal ice zones. Composites further reveal the presence of a tropopause polar vortex located above the Arctic cyclone but exhibiting a slight vertical tilt at the time of the ice loss event. Comparisons of Arctic

cyclones associated with very rapid ice loss events from those that are not reveal that cyclone lifetime, radius, and speed are statistically significant properties but minimum mslp is not.

Chapter 1

Introduction

1.1 Motivation

The Arctic is a dynamically changing environment, warming at approximately twice the rate as the rest of the world (e.g. Solomon et al. 2007; Blunden and Arndt 2012). One of the many consequences of accelerated warming in the Arctic is a dramatic reduction in both sea ice extent and thickness, particularly in the summer (Kwok and Cunningham 2010; Comiso 2012). This sea ice decline has resulted in more open ocean in this region than ever recorded, opening sea lanes not previously accessible (Stephenson et al. 2013; Stephenson and Smith 2015). These sea lanes make available the abundant natural resources of the Arctic. Accessing these newly available regions safely requires a thorough understanding of the hazardous ocean and weather conditions that occur there (Eicken et al. 2009; Lovecraft et al. 2013).

The Arctic's warming climate is also connected to an increase in the human populations in the region (Durkalec et al. 2015). These populations will be affected by coastal erosion, cyclone activity, and other climatological changes (Overeem et al. 2011; Dobrynin et al. 2012; Hemer et al. 2013; Barnhart et al. 2016). Ensuring the safety of the local populations and shipping workers during hazardous weather events requires reliable forecasting for the Arctic.

In addition to the concerns for Arctic stakeholders, a better understanding of the connection between cyclones and sea ice is critical for improving modeling capabilities. In some years a strong, long-lived cyclone can have dramatic affects on sea ice extent (SIE), such as the Great Arctic Cyclone of 2012 (Simmonds and Rudeva 2012). But most cyclones do not result in such dramatic ice loss. These differences provide a substantial challenge for seasonal prediction models' ability to forecast summer sea ice minimum extent (Stroeve

et al. 2015). In global climate models, even the most sophisticated do not capture current observed trends in Arctic cyclones (Nishii et al. 2015; Day et al. 2018) and consistently underestimate SIE decline (Msadek et al. 2014). By not being able to forecast sea ice loss from cyclones, models may be overestimating when an ice free September will occur.

1.2 Background

There are large bodies of work addressing Arctic cyclones and sea ice variability individually (e.g. Zhang et al. 2004; Serreze and Barrett 2008; Simmonds et al. 2008; Wang and Overland 2009; Sepp and Jaagus 2011; Wei et al. 2016) but fewer studies on the connections between the two. This section is divided into four parts: Arctic cyclones, Tropopause Polar Vortices (TPVs), sea ice, and cyclone-sea ice interactions. Our intent of this section is to provide sufficient background so that our hypotheses are appropriately framed within the broader context of past and current research into Arctic systems.

1.2.1 Arctic Cyclones

In this section we give an overview of Arctic cyclones. We address how Arctic cyclones are defined, seasonal and regional variability, and changes in Arctic cyclone properties over longer timescales, including teleconnections and climate variability.

There is no singular definition of an Arctic cyclone. The broadest definition is any cyclone that spends any amount of time north of 60°. The most restrictive definition classifies Arctic cyclones as long-lived, barotropic features that undergo both genesis and lysis over the central Arctic (Tanaka et al. 2012). Most studies use a definition closer to the former than the latter.

Whatever the specific definition, there are two broad categories that these cyclones fall into: cyclones that are born in the Arctic and cyclones that migrate in from the mid-latitudes. These categories are important because they have different seasonal and climatological variabilities (Sepp and Jaagus 2011). Additionally, cyclones entering from the

mid-latitudes tend to be stronger than those generated over the Arctic Ocean (Zhang et al. 2004). Many mid-latitude cyclones that migrate into the Arctic originate within the Icelandic Low (IL), where the strongest systems are found (Serreze et al. 1993).

Other complicating factors in discussing Arctic cyclones are differences in cyclone tracking algorithms and differing definitions for the Arctic itself. The southern border of the Arctic is generally taken to be between 60 and 70° N. While the choice of latitude is somewhat arbitrary it does affect how cyclones are divided between those two broad categories previously mentioned. Some of the main issues to come up with different tracking algorithms are whether vertical vorticity maxima or mean sea level pressure minima are tracked and whether the algorithm requires closed contours of the specified field to consider it a cyclone. For example, an algorithm that tracks vertical vorticity maxima may identify cyclogenesis before one that tracks sea level pressure minima (Mesquita et al. 2009; Neu et al. 2013; Rudeva et al. 2014).

Generally, there are fewer Arctic cyclones in the winter than there are in the summer and winter cyclones tend to be stronger than their summer counterparts (Zhang et al. 2004; Crawford and Serreze 2016; Day and Hodges 2018). There can be regional variations to that pattern. Winter is the more active season than summer for cyclones in the North Pacific, Bering Sea, and Alaska (Mesquita et al. 2010). Figure 1.1, taken from Zhang et al. (2004), shows cyclone counts for winter (Fig 1.1.a) and summer (Fig 1.1.b) from 1948 - 2002 and shows the seasonal differences in cyclone count location. Figure 1.1 also shows the long-term mean slp of cyclone centers for winter (Fig 1.1.c) and summer (Fig 1.1.d).

When strong, open systems which are not usually captured by tracking algorithms are included in cyclone counts, winter emerges as the most active season (Simmonds et al. 2008). Some of these inconsistencies can be attributed to differences in how an individual study defines the Arctic. However, despite these differences, there is general consensus in the literature that over the Central Arctic Ocean (CAO), there are fewer but stronger storms in the winter than the summer (Crawford and Serreze 2016).

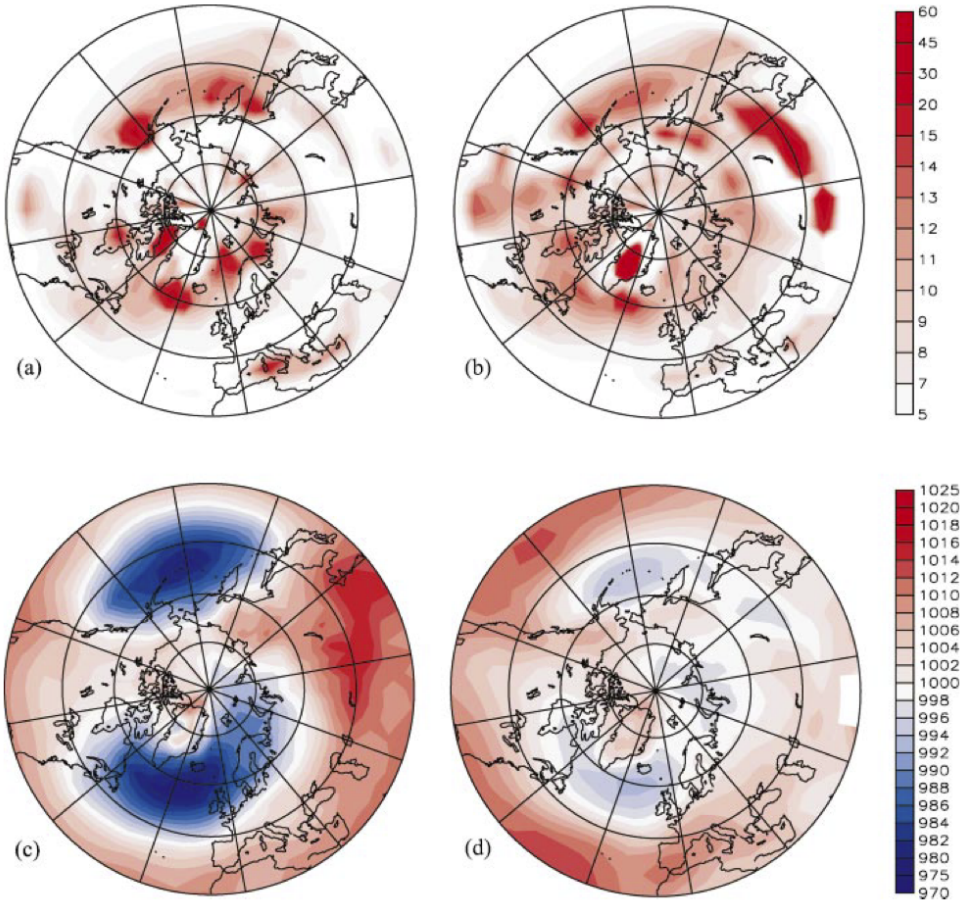

Figure 1.1: Figure 2 from Zhang et al. (2004). Winter (a) and summer (b) cyclone center counts (counts per 10^5 km^2). Panels (c) and (d) are winter and summer long-term mean SLP (hPa) respectively.

The Arctic frontal zone (AFZ) is a baroclinic region in the Arctic that is the result of the land-sea temperature contrasts along the Arctic coastline. It develops in the spring and persists through the summer as sea ice retreats and snow ashore melts (Reed and Kunkel 1960). Over the ocean, energy from the incoming solar radiation goes into melting sea ice and heating the upper layer of the ocean resulting in only small increases in air temperature. In contrast, air over the land increases quickly once the snow has melted.

It should be noted that in some places the term Arctic front and Arctic frontal zone are used to describe the boundary of the Arctic air mass. That feature exists year round but its border varies seasonally and geographically. It also roughly corresponds to the northern border of the boreal forest (Bryson 1965). While this air mass boundary is sometimes referred to as the Arctic front, it is a separate feature from the AFZ discussed here.

This region appears in the literature as early as 1945 (Dzerdzeevskii 1945) and was generally considered to be an important region for cyclogenesis (Reed and Kunkel 1960; Serreze et al. 2001; Serreze and Barrett 2008) based on the baroclinic instability model for genesis of extratropical cyclones (Eady 1949; Farrell 1985; Pierrehumbert and Swanson 1995). However, climatological studies indicate that in the summer, regions with the highest frequencies of cyclogenesis are to the south of the AFZ. More specifically, summer cyclogenesis favors the lee sides of the Verkhoyanski, Cherski, Gydan, and Mackenzie mountain ranges in Siberia and Alaska (Crawford and Serreze 2016). This led Crawford and Serreze (2016) to conclude that the AFZ plays a more important role in cyclone intensification than cyclogenesis.

There are additionally regional variations in cyclone frequency that themselves can vary seasonally. The North Atlantic storm track is a persistent region of both cyclogenesis and cycloysis in the North Atlantic Ocean and Greenland and Norwegian Seas, which is especially important in the winter (Serreze 1995). In the summer, additional regions of cyclogenesis are present over Siberia and Canada, as discussed in conjunction with the AFZ. Also note that the North Atlantic storm track is colocated with the IL, which is strongest in

the winter. Strengthening or weakening of the IL tends to correspond with strengthening and weakening of the Azores High. These patterns taken together are the North Atlantic Oscillation (NAO) (Walker 1923). A positive NAO is associated with an increase in cyclone activity in this region both in counts and intensity (Serreze et al. 1997).

No long term trend in the overall number of cyclones in the Arctic has been found (Screen et al. 2011; Simmonds et al. 2008; Serreze and Barrett 2008). There is evidence that the number of cyclones entering the Arctic is increasing, specifically through the Bering Strait, Alaska, the Baffin Sea, and Eastern Siberia but the number of cyclones formed over the CAO has remained constant (Sepp and Jaagus 2011). Cyclone counts, depth, and radius are connected to the Arctic Oscillation (AO) and to a somewhat lesser degree the NAO (Simmonds et al. 2008). The positive phase of the AO is associated with cyclones that are deeper, larger, and occur more frequently. Though the relationship between a positive AO and cyclone frequency and depth is stronger than the relationship with cyclone size (Simmonds et al. 2008).

1.2.2 Tropopause Polar Vortices

A tropopause polar vortex (TPV) is an extratropical feature based on the dynamic tropopause that can be either a cold-core cyclone or warm-core anti-cyclone. They are especially common in the Arctic because the polar environment is particularly conducive to sustaining vortices (Hakim 2000). A cyclonic TPV is characterized by a negative potential temperature anomaly, higher pressure and consequently a lower tropopause height. They are defined by a closed material contour and typically have a radius less than 1000 km. Additionally they can be incredibly long lived, with lifetimes capable of exceeding a month, making them the longest lived sub-synoptic scale atmospheric features on Earth (Cavallo and Hakim 2009, 2010).

TPVs play a role in the development and intensification of surface cyclones. The importance of tropopause disturbances in the development of synoptic scale surface cyclones

is well established (e.g. Eliassen and Kleinschmidt 1957; Hoskins et al. 1985). TPVs also have important implications for improving predictability in both the Arctic and mid-latitudes (Yamazaki et al. 2015; Cavallo et al. 2016). But here, we are primarily concerned with their connection to Arctic cyclones. A surface cyclone can form when a TPV passes over a temperature gradient at the surface, such as the AFZ or the sea ice margin.

1.2.3 Sea Ice

Arctic sea ice varies across many time scales. It has a strong annual cycle (freezing in the winter and melting in the summer) but there is also a significant amount of interannual variability. As the Arctic continues to warm at twice the rate as the rest of the planet (Solomon et al. 2007; Blunden and Arndt 2012), sea ice has declined in both thickness and extent (Comiso 2012). These differences are especially noticeable in September at the end of the melt season (Simmonds and Keay 2009). Even the most conservative estimates predict that this enhanced climate change will result in an ice free September this century (Stroeve et al. 2007; Boé et al. 2009; Wang and Overland 2009). However, as of the time of this writing, 2012 still holds the record minimum for September sea ice extent (Fetterer and Windnagel. 2017 to present, updated daily). Several mechanisms have been investigated to understand that interannual variability, including changes in cloud cover, wind, both atmospheric and oceanic heat transport, and cyclone activity (Kay et al. 2008; Schweiger et al. 2008; Wang and Overland 2009; Ogi et al. 2010; Graversen et al. 2011; Woodgate et al. 2010; Screen et al. 2011).

There are many ways in which a warming climate affects Arctic sea ice. Reduced sea ice extent is linked to increases in atmospheric and ocean mixed-layer temperatures (Stroeve et al. 2012), surface solar heating (Perovich et al. 2008), and ocean heat fluxes (Shimada et al. 2006; Woodgate et al. 2006; Steele et al. 2008).

Other ways in which the Arctic's rapidly changing climate affects sea ice are less intuitive than increasing temperatures. One example is the Atlantification of the Arctic Ocean.

The Arctic Ocean is fed by both the relatively cold, less saline Pacific waters and warmer Atlantic waters. One of the consequences of climate change in the Arctic is the Arctic Ocean becoming more like the Atlantic Ocean (Årthun et al. 2012). This means warmer ocean temperatures and an increase in near surface salinity, both of which can increase sea ice melt and inhibit sea ice growth (Lind et al. 2018). The length of the melt season is also increasing. This not only allows for more ice to melt but also reduces the amount of time sea ice has to recover before the next melt season (Markus et al. 2009). There has also been a decrease in the percentage of sea ice that persists from year to year, known as multi-year ice (Kwok and Cunningham 2010; Maslanik et al. 2011). Multi-year ice is thicker compared to first year ice and consequently harder to melt, meaning that current sea ice is more susceptible to large changes than in the past (Comiso 2012).

Some of the interannual variability can be attributed to the AO (e.g. Ogi and Wallace 2007; Knudsen et al. 2015). The AO tends to be in a negative phase in years where minimum sea ice extent is below the climatological trend. In negative AO years, there is a persistent positive potential temperature (θ) anomaly in the upper troposphere. When this anomaly is present in the late spring and early summer, there tend to be fewer clouds and fewer cyclones over the Arctic (Screen et al. 2011). That is, more clear-sky conditions, which allows for more direct sunlight on the sea ice.

1.2.4 Sea Ice and Cyclone Interactions

Much of the literature addressing connections between sea ice loss and Arctic cyclones is focused either on individual storms (e.g., Holt and Martin 2001; Simmonds and Keay 2009; Lammert et al. 2009) or overall trends in cyclone characteristics during anonymously high and low sea ice years (e.g., Simmonds and Keay 2009; Screen et al. 2011).

Perhaps the most well known cyclone associated with a large, sudden sea ice loss event is the Great Arctic Cyclone of 2012 (Simmonds and Rudeva 2012; Parkinson and Comiso 2013; Kriegsmann and Brümmer 2014). While the Great Arctic Cyclone is not the strongest

or longest lived storm recorded in the Arctic (Simmonds and Rudeva 2012), it was associated with 4.4% of the total decrease in sea ice extent that season, contributing to 2012's record minimum extent (Zhang et al. 2013).

There are several mechanisms by which an individual cyclone may affect sea ice. A cyclone can transport sea ice out of the Arctic through the Bering Straight or Barrents Sea and into lower latitudes where melt can more easily occur (Ogi and Wallace 2007; Ogi et al. 2008). Other mechanisms for sea ice melt have to do with the interplay between the atmosphere, ocean, sea ice. The marginal ice zone, the transitional region between open ocean and the solid sea ice pack, is frequently exposed to wind driven ocean waves and these coupled interactions have been the focus of a large body of research, both theoretically and practically (e.g. Wadhams 1981; Squire 2007; Asplin et al. 2012, 2014; Collins III et al. 2015). One such event was observed during a field campaign in 2009 by Asplin et al. where large ocean swells penetrated the sea ice pack up to 250 km from the edge, resulting in a significant size reduction of the ice floes (Asplin et al. 2012). Once the sea ice is mechanically broken into these smaller pieces, a greater area is exposed to heat fluxes causing it to be more susceptible to melt, especially in the summer months (Asplin et al. 2014). The sea ice margin is also a baroclinic zone which may contribute to local cyclongensis or strengthening, especially in the autumn (Overland and Wang 2010; Inoue and Hori 2011). Strong winds can induce upwelling, mixing warm ocean water up from beneath the freshwater cap and induce sea ice melt (Zhang et al. 2013).

Studies not focused on individual storms tend to address overall trends in cyclone characteristics during anonymously high and low sea ice years (e.g., Simmonds and Keay 2009; Screen et al. 2011). Years with anonymously low September sea ice extent tend to have fewer storms earlier in the summer than other years (Screen et al. 2011). There is no difference in the number of September cyclones between low and high sea ice years, but low sea ice years tend to have deeper and larger September cyclones than high sea ice years (Simmonds and Keay 2009).

Cyclones that occur in the late spring may act to preserve sea ice by increasing the cloudiness and consequently reducing melting from direct sunlight (Curry et al. 1993; Intrieri et al. 2002) and cyclones in the winter can sometimes increase the Arctic ice mass (Kriegsmann and Brümmer 2014), highlighting the complex nature of cyclone-sea ice interactions.

The primary goal of this thesis is to quantify the atmospheric conditions that proceed very rapid sea ice loss events (VRILEs). In order to accomplish that, we must first establish a specific definition for VRILEs to create a database of summer and winter events. Then we use compositing techniques to establish a relationship between the VRILEs and a surface cyclone paired with a TPV. Finally we characterize the unique properties of the cyclones associated with VRILEs, hypothesizing that long lived cyclones located over thin ice have the greatest impact on sea ice loss.

Chapter 2

Data and Methods

In this chapter, we describe the various methodologies used throughout this thesis. Section 2.1 address how VRILEs are defined and how their locations are identified. The next section, 2.2, details how we composite data for these events and how statistical significance of the composite mean fields are determined. In Section 2.3 we describe how individual surface cyclone tracks are paired with a VRILE and Section 2.4 provides information on how properties of those cyclones are determined to be significant or not.

2.1 Very Rapid Sea Ice Loss Events

VRILEs are large sea ice loss events unassociated with the intraseasonal cycle. The date and location of a VRILE are identified in two steps. First, daily sea ice extent data from National Snow and Ice Data Center (NSIDC) from 1979 - 2016 is used to find the daily change in sea ice extent. Then we use sea ice concentration data, also from NSIDC, to determine each VRILE's location (Fetterer and Savoie 2002). In identifying when VRILEs occurred, we first apply a three day running mean to the timeseries of daily changes in sea ice extent. At this point we consider two different methods of filtering to identify individual ice loss events. One is to remove a thirty year, climatological mean of those daily values. The second is to apply a Butterworth high-pass filter to remove any signal with a period greater than eighteen days. Eighteen days is chosen as the cut off based on maxima in the frequency spectrum of the smoothed, daily sea ice extent changes. For each of these definitions, VRILEs are taken to be the top 5% of loss events. Since there is no established definition for a VRILE, we use datasets of VRILEs based on both of these filtering methods and the combination of the two without overlap.

The methodologies described in the previous paragraph identify VRILEs in time but does not locate them in space. In order to know where VRILEs occurred we use sea ice concentration data also from NSIDC (Fetterer and Savoie 2002). We take the sea ice concentration from the dates previously identified and find the five day change in sea ice concentration. However, prior to 1988 sea ice concentration, data is only available every other day. For VRILEs that occurred between 1979 and 1987, a six day change in concentrations is used. Connected regions of negative change are identified and the largest region is taken to be the VRILE. Whenever possible the entire loss object is considered but when a single point is required for the VRILE location, the point within the loss object with the greatest negative change in sea ice concentration is used.

2.2 Composite Means

VRILEs can occur anywhere there is sea ice, in the Arctic Ocean itself and further south into Hudson Bay. Consequently, care must be taken when creating composites because we are not identifying the mean state of a specific location but rather the mean state of the atmosphere for a type of event. We consider composites centered on three different locations: the VRILE itself, the closest local minima in mean sea level pressure (mslp) to the VRILE location, and the closest local minima in θ to the VRILE on the dynamic tropopause, taken to be the 2 PVU ($10^{-6} m^2 sec^{-2} K kg^{-1}$) surface.

To make composite images centered on the VRILE, we take the point within the loss object with the greatest negative change in sea ice concentration as the center of a 6000 x 6000 km box. The data in that box are then projected onto an evenly spaced 30 km grid. 30 km is chosen to correspond to the 25 km grid spacing of the sea ice concentration data. This process is identical for the different center points. The composite means are taken on the day of the VRILE and daily time lagged composites back to five days before the event. Time lagged composites are only presented for the Butterworth filter VRILE definition. The method of filtering did not produce noticeably different results in the composite

means. The Butterworth filter definition is chosen over the other two because by design it identifies ice loss events that occur over a short period of time. The purpose of this thesis is to understand those short-term atmospheric conditions surrounding VRILEs, making the Butterworth filter definition the natural choice.

The fields we composite are standardized anomalies in mslp and θ on the dynamic tropopause. The units for both fields are standard deviations. Mslp is contoured every half σ from -3 to 3. The θ standardized anomalies are shaded for -3 to 3 σ such that negative anomalies are blue and positive anomalies are red. Data for these composites come from ERA-Interim (ERA-I) reanalysis (Dee et al. 2011) and unless otherwise noted data from 0Z is used. Anomalies are relative to ERA-I monthly mean values from 1981-2010. For the time lagged means centered on the VRILE, the center of the composites remains the same and only the atmospheric data change. When centered on local mslp or θ minima, the center is recalculated at each timestep.

Measuring the statistical significance of the composite means presents a challenge for the same reasons care had to be taken when creating the composites themselves. The features we are interested in occur nonuniformly in both space and time. Testing the statistical significance of any signal is predicated on establishing an appropriate null hypothesis. In this instance, our null hypotheses are that the mslp and tropopause θ are not significantly different from average conditions. Therein lies a complication of the nonuniformity of VRILEs because that normal state is also a function of space and time.

In order to establish what that normal state is which to compare our composites, we generate random datasets. This process begins by choosing a random location in the Arctic. Our only requirements are that the point to be north of 55° and not over land. 55° is chosen as the southern boundary so that typical conditions for non-Arctic VRILEs, such as those occurring in Hudson Bay, are included in the dataset. Then a random day is selected. Separate datasets are made for summer and winter. For the summer dataset, valid dates are June to August 1979 - 2016. Similarly, the valid dates for winter are December through

February 1979 - 2016. These points are used to create the same type of 6000 square km datasets used in the composite means. Each dataset contains 5000 members.

With these datasets in hand, we use bootstrap re-sampling to determine statistical significance. We create a probability distribution for each point in our grid-space by randomly selecting a subset of the random dataset equal to the corresponding number of VRILEs and taking the mean. That process is repeated 10,000 times, creating a probability distribution for the mean value at each location in the map space. We compare the value in our composite mean to these distributions and consider our signal to be statistically significant if it falls within the 99^{th} percentile of that distribution. Statistical significance is indicated on the composite figures with grey stippling. Only one field's statistical significance, mslp or θ on the dynamic tropopause, is shown at a time.

2.3 Cyclone Track Matching

The second approach we take to quantifying the atmospheric conditions preceding the sea ice loss is to identify Arctic cyclones associated with each VRILE. Here we consider any cyclone that spends any amount of time north of 60°. This broad definition of an Arctic cyclone is used because many several VRILEs occur south of 60°, such as Hudson Bay events. Consequently any more restrictive definition tends to exclude surface cyclones associated with VRILEs. We consider a cyclone to be associated with a VRILE if the center of the cyclone passes within a certain distance of any point within the VRILE no more than five days before it occurred. Five days is chosen for consistency with the methodology for VRILE detection described earlier in Section 2.2. The distance cutoff is chosen based on a composite comparison of the sea ice loss objects and cyclone locations. We use cyclone tracks derived from the joint reanalysis product from the National Centers for Environmental Prediction and National Center for Atmospheric Research (NCEP/NCAR) (Serreze 2009) as well as the European Centre for Medium-Range Weather Forecasts interim reanalysis product (ERA-I) (Hanley and Caballero 2012).

To create the composite of the ice loss objectes identified in the sea ice concentration data, the objects are projected in the same manner as before. We then take the sum of the data instead of the mean because the ice loss objects are stored as masks. That is, if a grid point is within the object, it is flagged with a one and otherwise the grid point is flagged with a zero. The composites are also centered on the point within each loss object that contained the greatest negative change.

We then identify any cyclone in the NCEP/NCAR track list that passes within 2000 km of any point within that loss object no more than five days before the event. We choose 2000 km simply as an upper bound. Only NCEP/NCAR cyclone tracks are used at this stage because the ERA-I list does not go back to 1979. The locations of those cyclones that fall within the five day cutoff are projected onto the evenly spaced map and each of those points is plotted along with the composite loss object.

2.4 Cyclone Properties

The method described above produces two subsets of each track list: cyclones associated with VRILEs and those that are not. We do this by creating probability density functions for each of the properties of interest. These properties are cyclone lifetime, radius, strength in terms of minimum mslp, pressure gradient, and speed. For the cyclones associated with a VRILE, we consider these properties, with the exception of lifetime, both for the entire lifetime of the cyclone and restricted to the five days before the VRILE. The statistical significance of each of the properties is determined by using a Kolmogorov–Smirnov (K-S) test. The K-S test is a nonparametric test of statistical significance. Its null hypothesis for a two sample test is that both samples were drawn from the same distribution. We consider the two distrubutions to be significantly different if $p \leq 0.01$.

Part of our hypothesis regarding the ideal conditions for a VRILE to occur is that thin ice is more susceptible to large, sudden loss events than thicker ice. Of all the mechanisms described in Section 1.2.4, wind driven ocean waves in the marginal ice zone breaking up

large ice floes into smaller ones seems to be the most likely candidate for causing VRILEs. As observed by Asplin et al. (2012), the small ice floes can melt rapidly, a necessary condition for a VRILE to occur. Characterizing the ice conditions that a particular cyclone interacts with is not straight forward. We approach this issue by considering the minimum distance the cyclone is from the 15% sea ice concentration contour (Zwally et al. 1983). Sea ice concentration is not a direct corollary for sea ice thickness. However, a database of sea ice thickness for the entire Arctic sea ice mass from 1979 - 2016 does not currently exist and so we use sea ice concentration as a proxy. We use the cyclone location and sea ice concentration data from the day the VRILE occurred. If on the day the VRILE occurred the cyclone location does not meet the criteria to be considered associated with the VRILE then the cyclone location closest in time that does meet the distance criteria is used.

Chapter 3

Very Rapid Sea Ice Loss Events

There are advantages and disadvantages to each of the definitions discussed in Section 2.1. For the mean removed, we expect there to be more VRILEs later in time due to the strong climatological trend in SIE. Removing the climatological mean (1981 - 2010) in daily sea ice extent highlights loss events which are large relative to that mean state. Given the rapid decline in sea ice extent over that period, the largest changes compared to that mean would likely occur later. As for the Butterworth filter definition, it will filter out any long term trends in the frequency of VRILEs.

This process results in three sets of VRILEs for both summer and winter: VRILEs identified by the Butterworth filter, those identified by removing the climatological mean, and those two categories combined without double counting events. We additionally control for events identified on consecutive days in order to ensure that each VRILE is a unique event. The number of VRILEs identified in those three categories for both seasons are presented in Table 3.1.

In the winter, every VRILE identified by the mean removed definition is also identified by the Butterworth filter definition. Consequently the list of VRILEs in the "All" category in winter is identical to "Butterworth Filter" list. This is not the case in the summer. For

	Butterworth Filter	Mean Removed	All
Summer (1979 - 2016)	76	92	133
Winter (1979 - 2016)	141	117	141

Table 3.1: Number of VRILEs identified by applying a Butterworth filter, removing the climatological mean, and the combined total of both methods without overlap for summer (JJA) and winter (DJF) months.

the summer months, there were VRILEs identified by the mean removed definition not identified by the Butterworth filter definition and vice versa. The 24 winter VRILEs only identified by the Butterworth filter all occurred between 1979 and 1990. In the summer, we also see that generally, the VRILEs identified by using a Butterworth filter and not by removing the mean occurred before 2000. While there are summer VRILEs identified solely by the mean removed definition as early as 1979, the majority of them are in the later half of the time period.

These outcomes are consistent with our expectations of both filtering methods. VRILEs identified by removing the climatological mean are skewed towards the later half of the time period, capturing climatological decreases in sea ice extent. Events identified by the Butterworth filter are more evenly distributed with time as any trend in sea ice extent that occurs over more than 18 days is removed.

3.1 VRILE Locations

In both summer and winter, VRILE locations generally located in the vicinity of the sea ice edge. The locations are unsurprisingly further south in the winter than the summer, reflecting differences in seasonal sea ice extent. In addition to clustering around the sea ice edge, winter VRILE locations include a semi-linear feature that extends from just North of Iceland across the Barents Sea (Figure 3.1.a). This pattern at least visually coincides with the North Atlantic storm track and the Icelandic Low. There is also a cluster of VRILEs south of the Bering Strait. While this location corresponds to the seasonal sea ice edge, it could also be capturing transport of sea ice through Bering Strait (Figure 1.1.a and Figure 3.1.a, c, and e).

Summer VRILEs are further north than their winter counterparts. Given that Hudson Bay is ice free by the end of the summer, seeing large grouping of ice loss events there is unsurprising. The other summer VRILEs tend to be northward of the Siberian and Alaskan

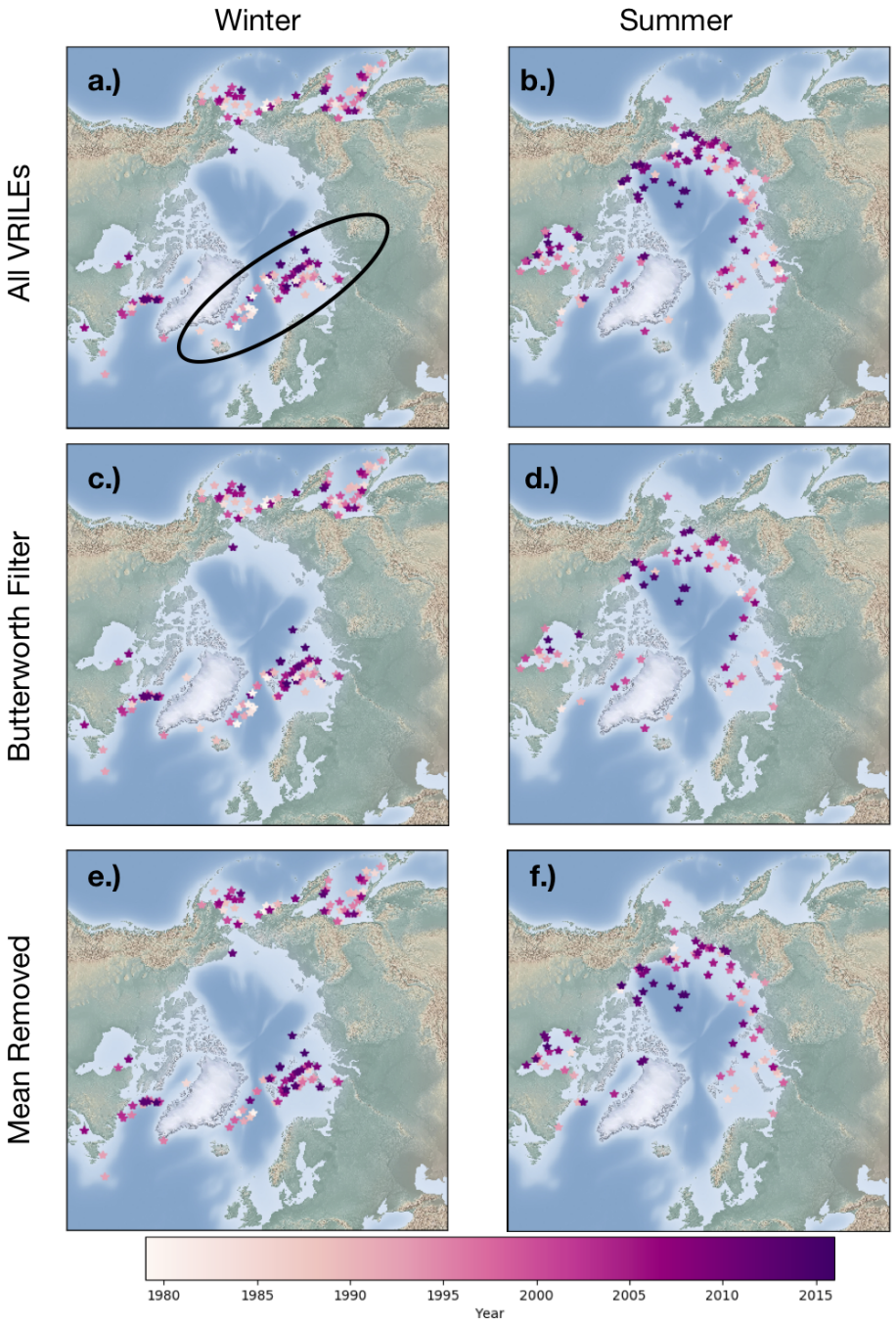

Figure 3.1: Identified locations of VRILEs are marked with stars for winter (left column) and summer (right column) events. Panels (a) and (b) are the combination of both the Butterworth filter and mean removed definitions for VRILEs. Panels (c) and (d) represent the Butterworth filter definition. Panels (e) and (f) are for the mean removed definition. Winter VRILE locations in the North Atlantic storm track are circled in panel (a). Locations are color coded by the year they occurred.

coastlines, roughly corresponding to summertime storm tracks associated with the AFZ (Figure 1.1.b and Figure 3.1.b, d, and f).

Chapter 4

Atmospheric Conditions Preceding VRILEs

As previously stated, one of the goals of this thesis is to establish a relationship between VRILEs and a preceding arctic cyclone. The aim of this chapter is to identify the atmospheric conditions surrounding VRILEs. We approach this question from three directions. First we analyze a case study of a VRILE from August 7^{th}, 2008. The second is a composite sense. That is, we take the composite mean of standardized anomalies of various fields at and around the VRILE locations discussed in Chapter 3. The third approach is to use cyclone tracks derived from different reanalysis products and compare their locations with VRILEs to identify individual cyclones associated with individual VRILEs.

4.1 August 7^{th}, 2008 Case Study

In order to highlight the methods used in this section, we begin with a single VRILE that occurred on August 7^{th}, 2008. This case is chosen because this particular event has not been studied in existing literature and is one of the smaller events. This VRILE is associated with a loss of -0.14 km^2 of sea ice. The average sea ice loss for a summer VRILE is -0.168 km^2, after the butterworth filter is applied.

The VRILE location is near the coast, southeast of Wrangel Island (Figure 4.1.a). The entire sea ice loss object identified in the five day concentration change is an elongated, irregular shape off the coast of Siberia (Figure 4.1.b). At first glance, the shape of the VRILE seems odd. Is this truly, physically a single ice loss event or was it only identified as an individual event because of the criteria of our identification system?

Three cyclones from the NCEP/NCAR reanalysis cyclone track list pass within 1000 km of the object within five days of the VRILE. Those tracks are plotted in Figure (4.1.b). The longest lived of the three wraps around nearly the entirety of the loss object. The

presence of this cyclone quells some of our earlier concerns regarding the validity of the location identification because one ice loss event is corresponding to one cyclone. The other two, shorter lived cyclones may have had more local affects on the tail of the loss object.

Figure 4.2 shows the time evolution of both potential temperature on the dynamic tropopause and mslp in the five days proceeding the VRILE. For reference, the sea ice loss object and cyclone tracks from Figure 4.1.b are included in each panel.

Following the longest lived of the three cyclones through time, we see that it is paired with a TPV. By August 4^{th}, the surface cyclone has wrapped in the TPV and the two are roughly vertically aligned from the 5^{th} forward. Note that the mslp and θ data comes from ERA-I reanalysis data while the plotted cyclone tracks are derived from NCEP/NCAR reanalysis. Even so, the locations from the tracks are well aligned with the surface cyclone observable in the mslp data.

Another interesting feature in Figure 4.2 is the interaction between the three cyclones. At the time the VRILE occurred, the longest lived cyclone is over the Arctic ocean and one of the shorter lived cyclones is on the opposite side of the loss object, over land in Siberia. It is somewhat difficult to differentiate the two shorter cyclones in the mslp data, but there is at least one present on the 7^{th}. The combination of affects from these cyclones is potentially increasing the strength of the pressure gradient across the sea ice and consequently increasing wind speed as well. As discussed previously, the primary ways surface cyclones have been observed to affect sea ice are wind driven ocean waves and vertical mixing.

4.2 Composite Data

4.2.1 Composite Means

In this section, we use composite means of standardized anomalies of mslp and θ on the dynamic tropopause, described in Section 2.2, to test the hypothesis that cyclones coupled with TPVs proceed VRILEs. We center the composites on the VRILE locations and local

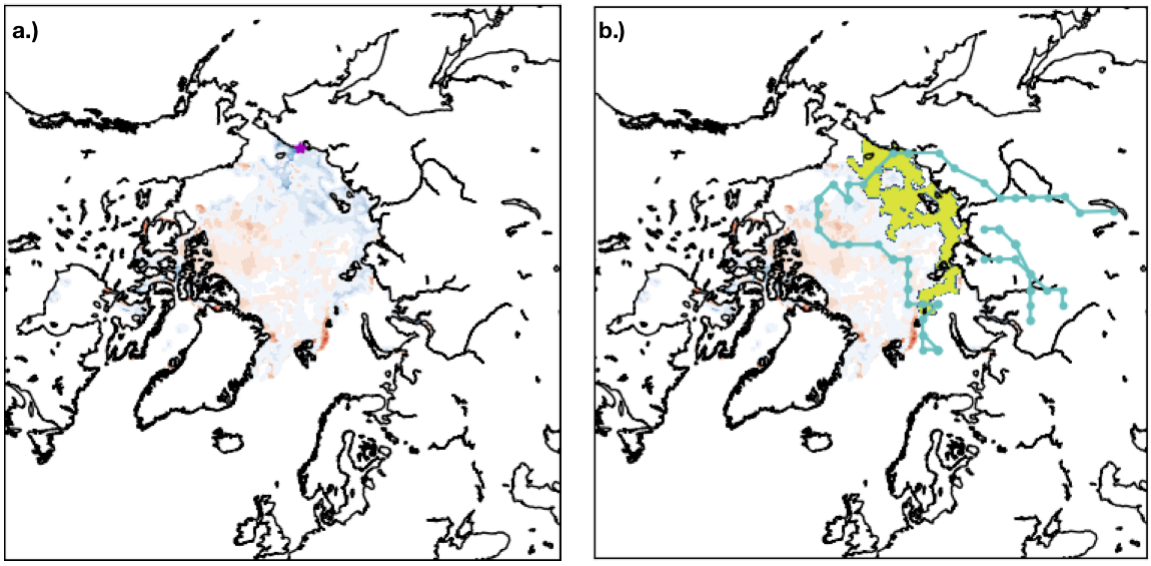

Figure 4.1: Change in sea ice concentration between August 7^{th} and 2^{nd} is shown as the color contours in both panels. Blue represents negative change and red positive. The location of the VRILE is marked by the magenta star in panel (a), which represents the point within the largest connected region of loss that experienced the greatest negative change in sea ice concentration. The yellow region in panel (b) shows the entire loss object and the cyclone tracks from NCEP/NCAR reanalysis associated with the VRILE are plotted in cyan.

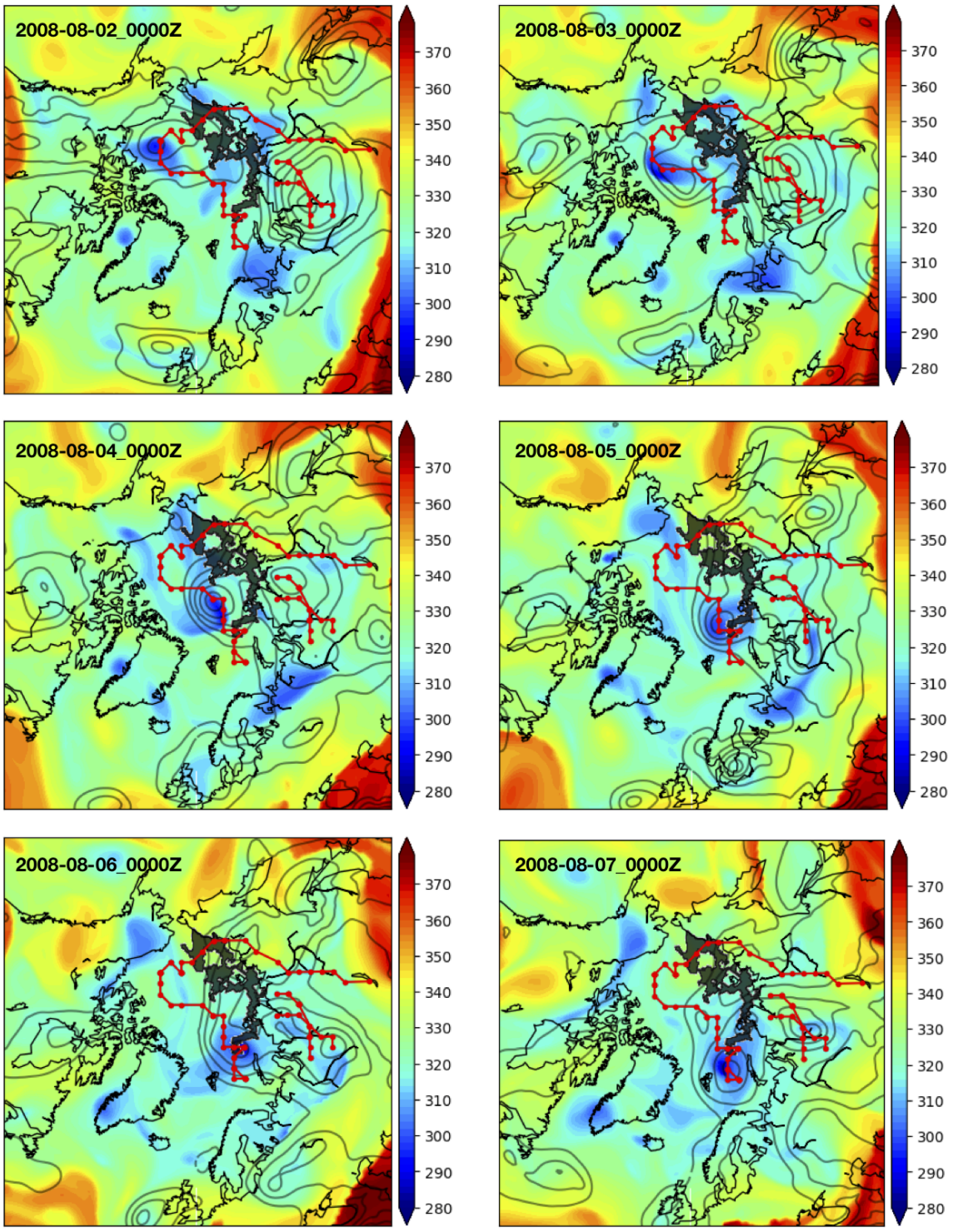

Figure 4.2: Time evolution of potential temperature on the dynamic tropopause, in Kelvin, shown as the color fill and mslp, represented by the grey contours every 5 hPa from 1010 to 950 hPa. The dark grey shaded region is the sea ice concentration loss object, and the red curves are surface cyclone tracks, as in Figure 4.1.b.

minima in mslp and θ on the dynamic tropopause. All three of the definitions of VRILEs presented in the previous chapter are used for robustness.

In Figure 4.3, the composite means are centered on the VRILEs, organized by the definitions from Table 3.1 and season. Statistical significance of the mslp field is shown. Figure 4.3.a and 4.3.b are composited over all VRILEs for winter and summer months respectively. Figure 4.3.c and 4.3.d only use data for VRILEs identified by the Butterworth filter and 4.3.e and 4.3.f only use data for VRILEs identified by removing the climatological mean.

There are two notable features in this figure. First is the change in sea level pressure across the VRILE. The change in standardized anomalies is about two standard deviations regardless of season or VRILE definition. Each of these pressure centers is statistically significant. The weakest pressure change is observed in the summer, mean removed composite (Figure 4.3.f). There is also a positive θ anomaly on the dynamic tropopause approximately centered over the VRILE which is stronger in the winter than the summer.

Figure 4.4 is organized in the same manner as Figure 4.3, with 4.4.a and 4.4.b showing all VRILEs, 4.4.c and 4.4.d for the Butterworth filter definition, and 4.4.e and 4.4.f for mean removed. Statistical significance is also shown for mslp. However here the composite is centered on the closest minima in mslp to the VRILE.

As with the VRILE centered composites, there are not significant differences between the different VRILE definitions. All show a distinct cyclone signal with a central pressure at least three standard deviations below the mean. The winter cyclones tend to have a larger radius than their summer counterparts. There is also a negative θ anomaly on the tropopause, indicative of a TPV (Cavallo and Hakim 2010), whose center is slightly offset from the center of the cyclone. This negative anomaly is paired with a positive θ anomaly, forming a dipole signal. That dipole signal is stronger in the winter than in the summer.

For Figure 4.5, the composites are centered on the local θ minima on the dynamic tropopause and statistical significance is shown for θ. The panels are arranged with 4.5.a

and 4.5.b composited over all VRILEs, 4.5.c and 4.5.d composited over the Butterworth filter definition of VRILEs, and 4.5.e and 4.5.f composited over the mean removed definition. We see effectively the same patterns here as we did in Figure 4.4, with a dipole signal in θ on the tropopause and the TPV center offset from the surface cyclone center. This pattern is present in both winter and summer and for all VRILE identification methods, though the signal is stronger in the winter.

The main take away from the data in Figures 4.3, 4.4, and 4.5 is the presence of a surface cyclone. No matter which particular definition for a VRILE we use and regardless of season, the composite means persistently show an Arctic cyclone associated with the VRILEs. In Figure 4.3 the presence of the cyclone is seen in the pressure change across the VRILE. Recentering the composites on mslp minima in Figure 4.4 reveals a clearer picture of the cyclone itself. Additionally we see in Figures 4.4 and 4.5 that the cyclone is paired with a TPV and that both the TPV and surface cyclone signals are statistically significant.

Figures 4.6 and 4.7 are winter, composite means centered on the VRILE location for the five days before the VRILE. For both figures, panel (a) is for the day of the VRILE, panel (b) shows data from the day before VRILE, and so forth to panel (f) which shows data five days before the VRILE. The only difference between Figure 4.6 and 4.7 is that Figure 4.6 shows the statistical significance of the mslp field and Figure 4.7 shows the statistical significance of the θ field.

The most striking feature in Figure 4.6 is that the change in surface pressure across the VRILE is greatest the two days before the VRILE (Figure 4.6.c). The dipole signal in mslp standardized anomalies does not dissipate until five days before the VRILE, though it is noticeably weaker four days before (Figures 4.6.e and 4.6.f). The positive θ anomaly on the tropopause does not exhibit that same behavior. That signal weakens quickly, becoming indistinguishable from the background flow by the fourth day (Figure 4.7.e).

Figures 4.8 and 4.9 are identical to Figures 4.6 and 4.7 except that they are for the summer months rather than winter, with panels (a) - (f) referring to days 0 to -5 relative to the

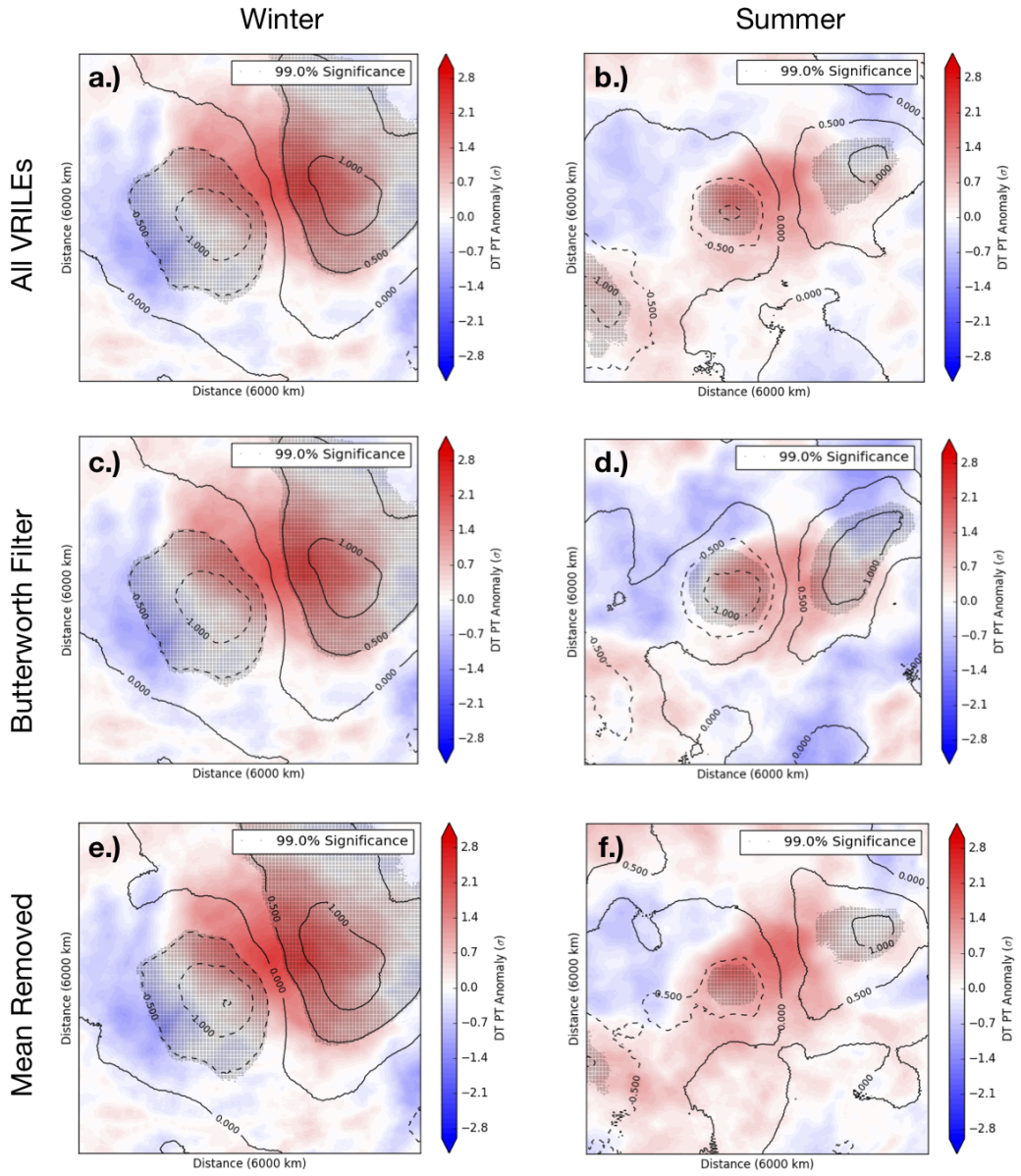

Figure 4.3: Composite means of standardized anomalies of mslp, represented by the black contours, and θ on the 2 PVU surface, represented by the shaded background, centered on the VRILE location. Both fields are shown from -3 to 3 σ with mslp contoured every 0.5σ. Grey stippling indicates statistical significance of the mslp field at the 99% level. Panels (a) and (b) use the combined list of VRILEs from both filtering methods for winter and summer month respectively. Panels (c) and (d) are composited only for the Butterworth filter definition of VRILEs and panels (e) and (f) use only the mean removed definition, with panels (c) and (e) composited over the winter events and panels (d) and (f) composited over summer events.

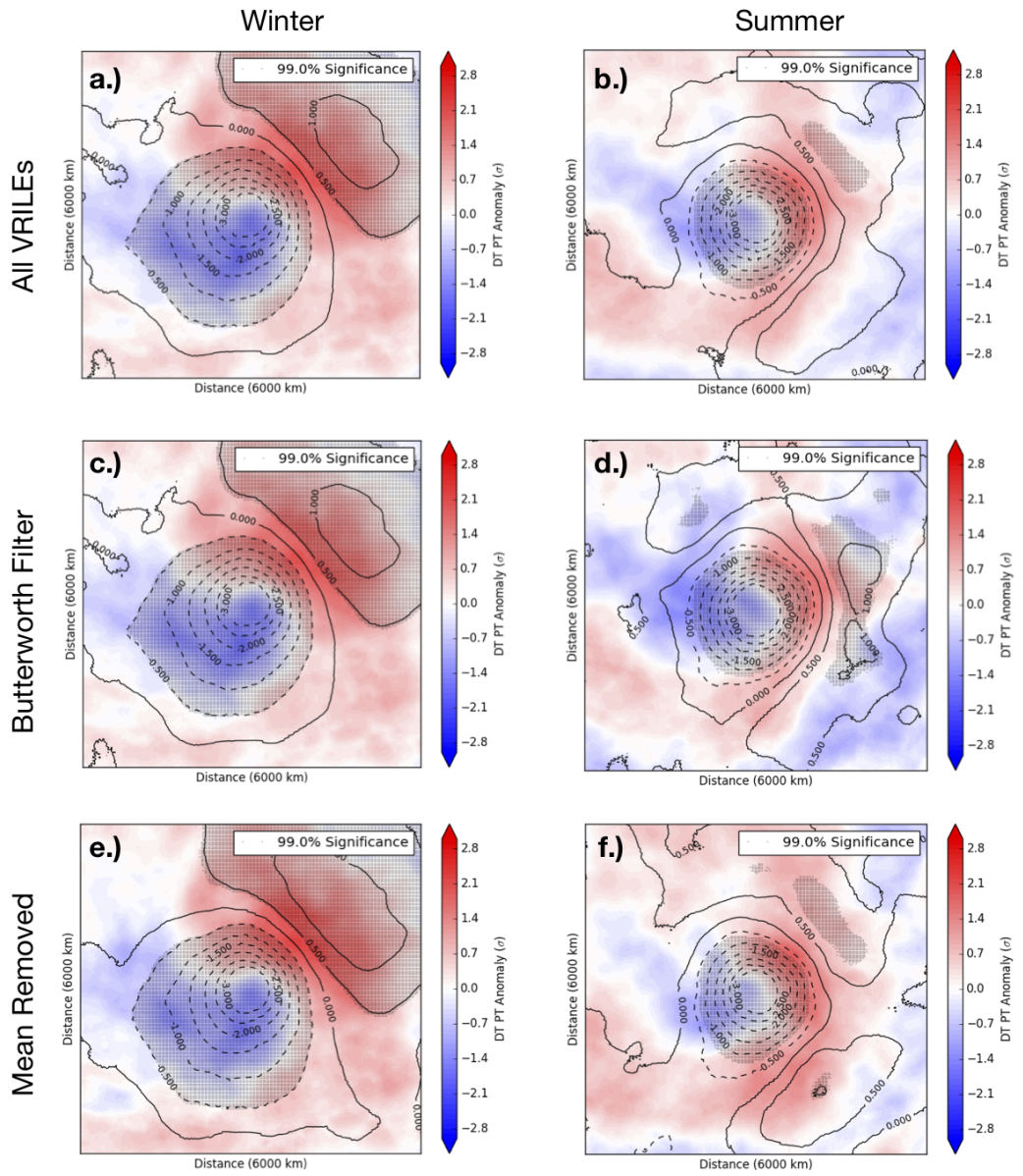

Figure 4.4: Composite means of standardized anomalies of mslp, represented by the black contours, and θ on the 2 PVU surface, represented by the shaded background, centered on the closest mslp minima to the VRILE. Both fields are shown from -3 to 3 σ with mslp contoured every 0.5σ. Grey stippling indicates statistical significance of the mslp field at the 99% level. Panels (a) and (b) use the combined list of VRILEs from both filtering methods for winter and summer month respectively. Panels (c) and (d) are composited only for the Butterworth filter definition of VRILEs and panels (e) and (f) use only the mean removed definition, with panels (c) and (e) composited over the winter events and panels (d) and (f) composited over summer events.

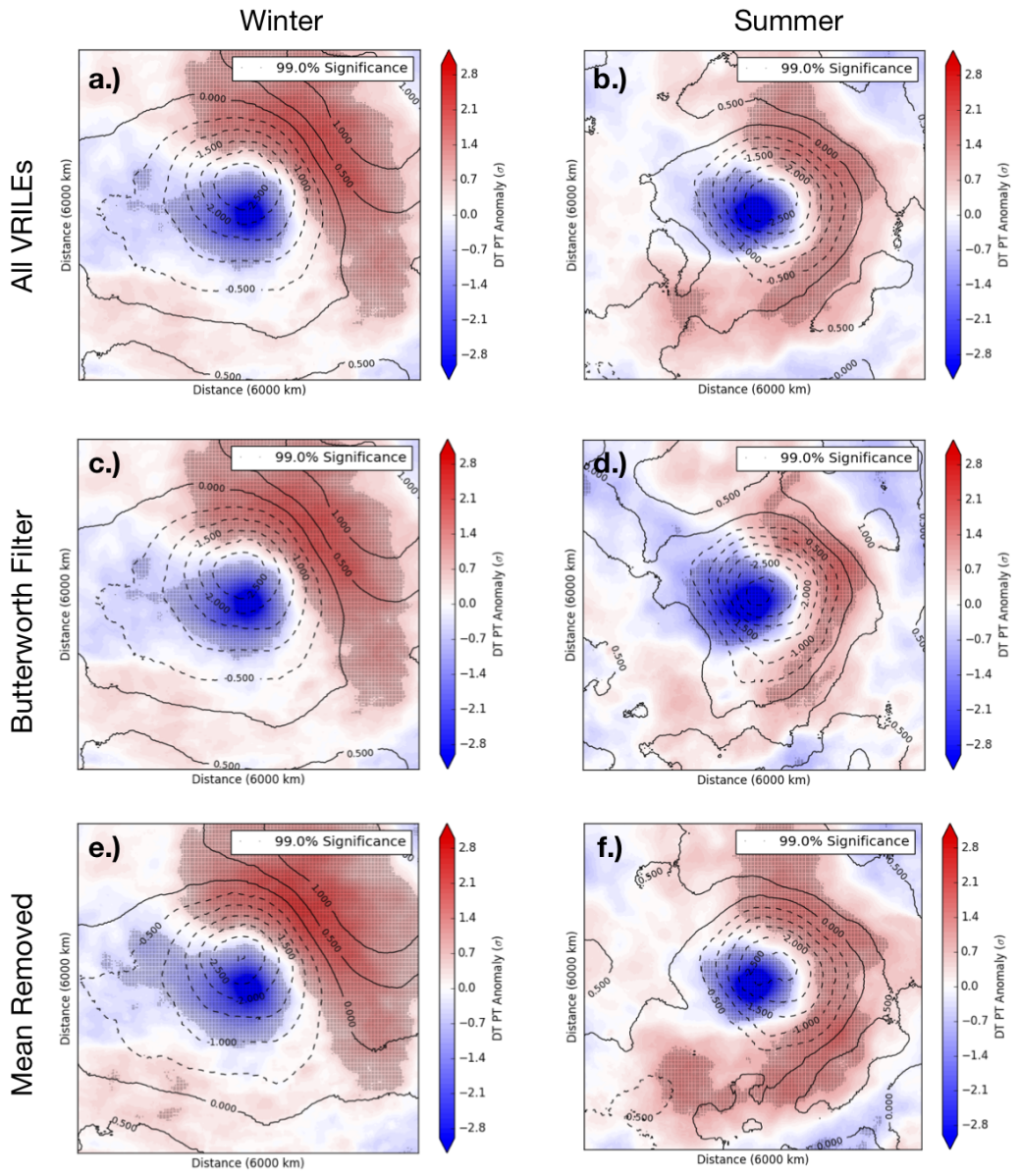

Figure 4.5: Composite means of standardized anomalies of mslp, represented by the black contours, and θ on the 2 PVU surface, represented by the shaded background, centered on the closest θ minima to the VRILE. Both fields are shown from -3 to 3 σ with mslp contoured every 0.5σ. Grey stippling indicates statistical significance of θ on the 2 PVU surface at the 99% level. Panels (a) and (b) use the combined list of VRILEs from both filtering methods for winter and summer month respectively. Panels (c) and (d) are composited only for the Butterworth filter definition of VRILEs and panels (e) and (f) use only the mean removed definition, with panels (c) and (e) composited over the winter events and panels (d) and (f) composited over summer events.

date of the VRILE. In the summer, both the mslp and θ signals break down quickly. There is no increase in the mslp gradient as there was in winter and there is no distinguishable signal in mslp or θ by day three (Figure 4.9.d).

There are notable differences between the summer and winter signals in the VRILE centered composites. These differences may point to the relative importance of dynamic versus thermodynamic forcings between the seasons. The winter, lagged composite centered on the VRILE (Figure 4.6.c) may indicate some form of dynamic preconditioning of the sea ice occurs to allow the sudden, dramatic ice loss required for a VRILE. One example of a dynamic preconditioning process is wind driven, ocean waves intruding into the marginal ice zone which break up ice floes, such as the processes observed by Asplin et al. (2012). However, in the summer the mslp signal is strongest the day of the VRILE (Figure 4.8.a). This may indicate that there are other mechanisms acting on the sea ice in the summer, conditioning the sea ice to allow a VRILE, that are not at play in the winter. For example, late spring and early summer with clearer skies tend to proceed low September sea ice years (Screen et al. 2011). Direct sunlight on the ice can lead to thinner ice, potentially more susceptible to cyclone induced losses. That type of thermodynamic preconditioning on the sea ice is not possible in the winter due to long periods without sunlight. The relative importance of dynamic versus thermodynamic forcings on sea ice, how those forcing vary with time, in terms of both season and climate change, and the implications for sea ice forecasting are interesting avenues of future analysis. However those questions are beyond the scope of this thesis.

Figures 4.10 and 4.11 are time lagged composites centered on the mslp minima for winter and summer respectively with panels (a) - (f) corresponding to days 0 to -5 days before the VRILE. To create the time lagged composites, the location of the local minima is recalculated for each day. This is akin to tracking the cyclone back in time. In both seasons the strength of the cyclone only decreases slightly over the five days. However, the size of the cyclone noticeably diminishes. In both seasons the strength of the TPV

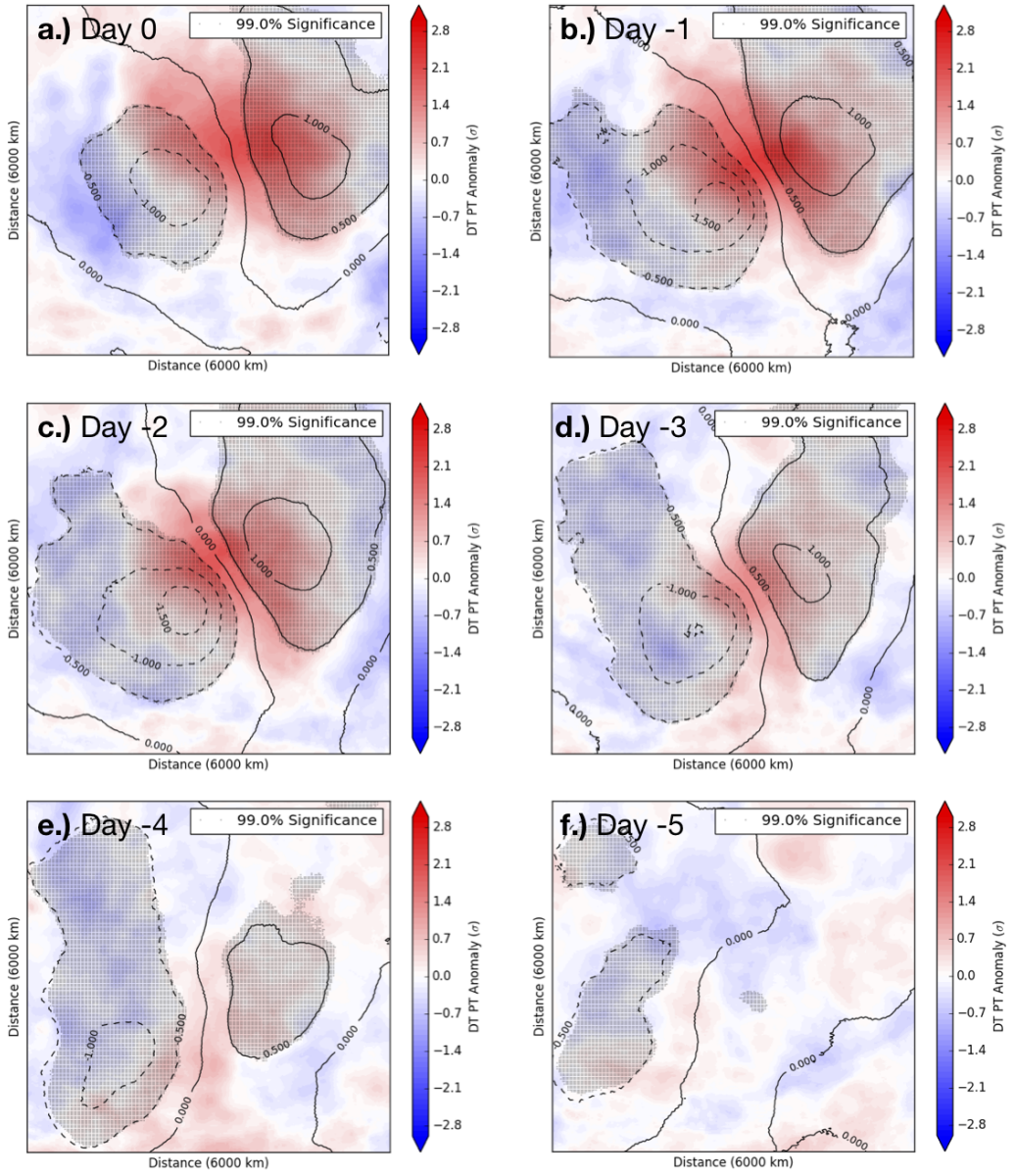

Figure 4.6: Winter, time lagged, composite means of standardized anomalies of mslp, represented by the black contours, and θ on the 2 PVU surface, represented by the shaded background, centered on the VRILE location. Both fields are shown from -3 to 3 σ with mslp contoured every 0.5σ. Grey stippling indicates statistical significance of the mslp field at the 99% level. Panels (a) - (f) correspond to day 0 to -5 relative to the VRILE.

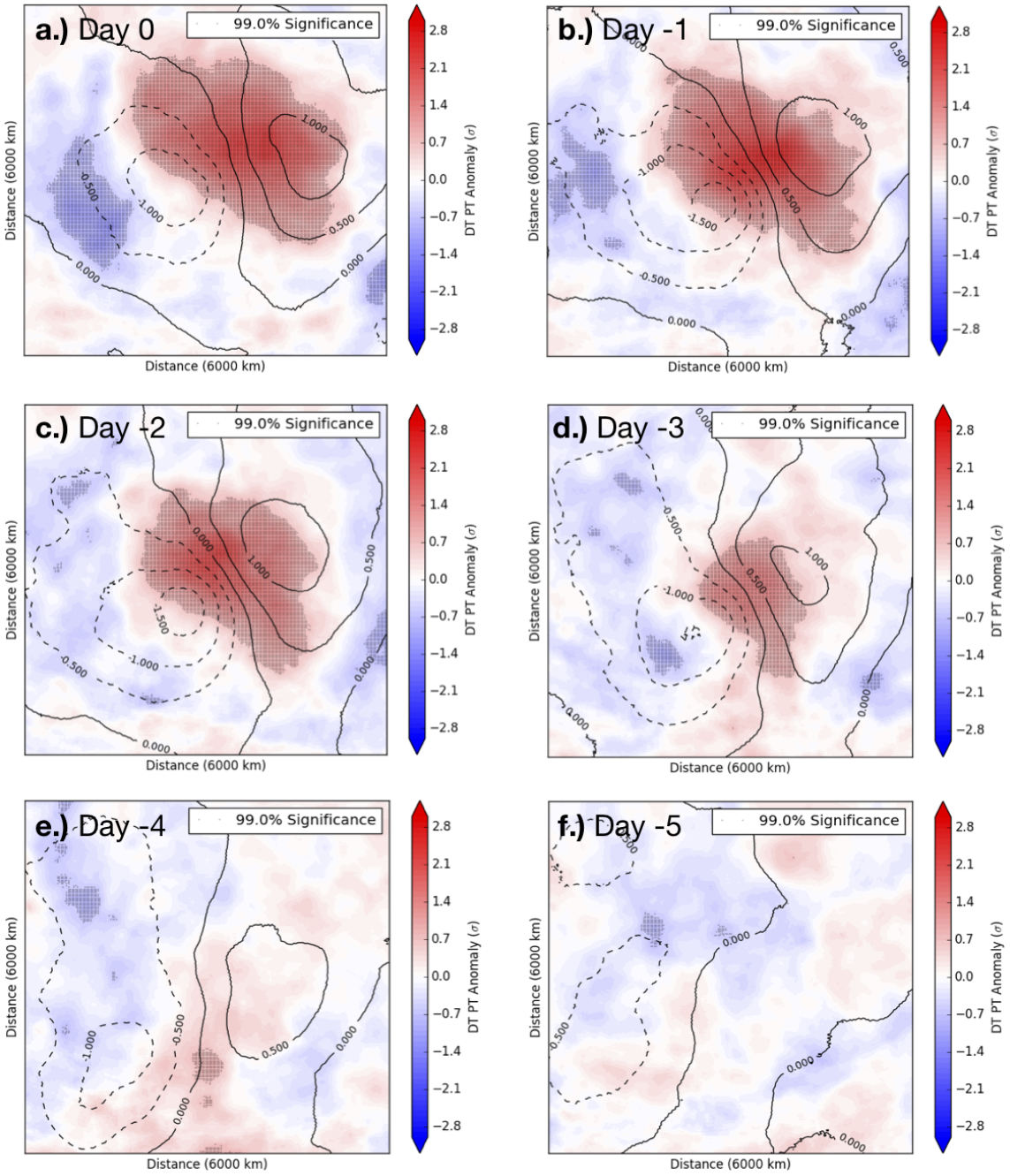

Figure 4.7: Winter, time lagged, composite means of standardized anomalies of mslp, represented by the black contours, and θ on the 2 PVU surface, represented by the shaded background, centered on the VRILE location. Both fields are shown from -3 to 3 σ with mslp contoured every 0.5σ. Grey stippling indicates statistical significance of θ on the 2 PVU surface at the 99% level. Panels (a) - (f) correspond to day 0 to -5 relative to the VRILE.

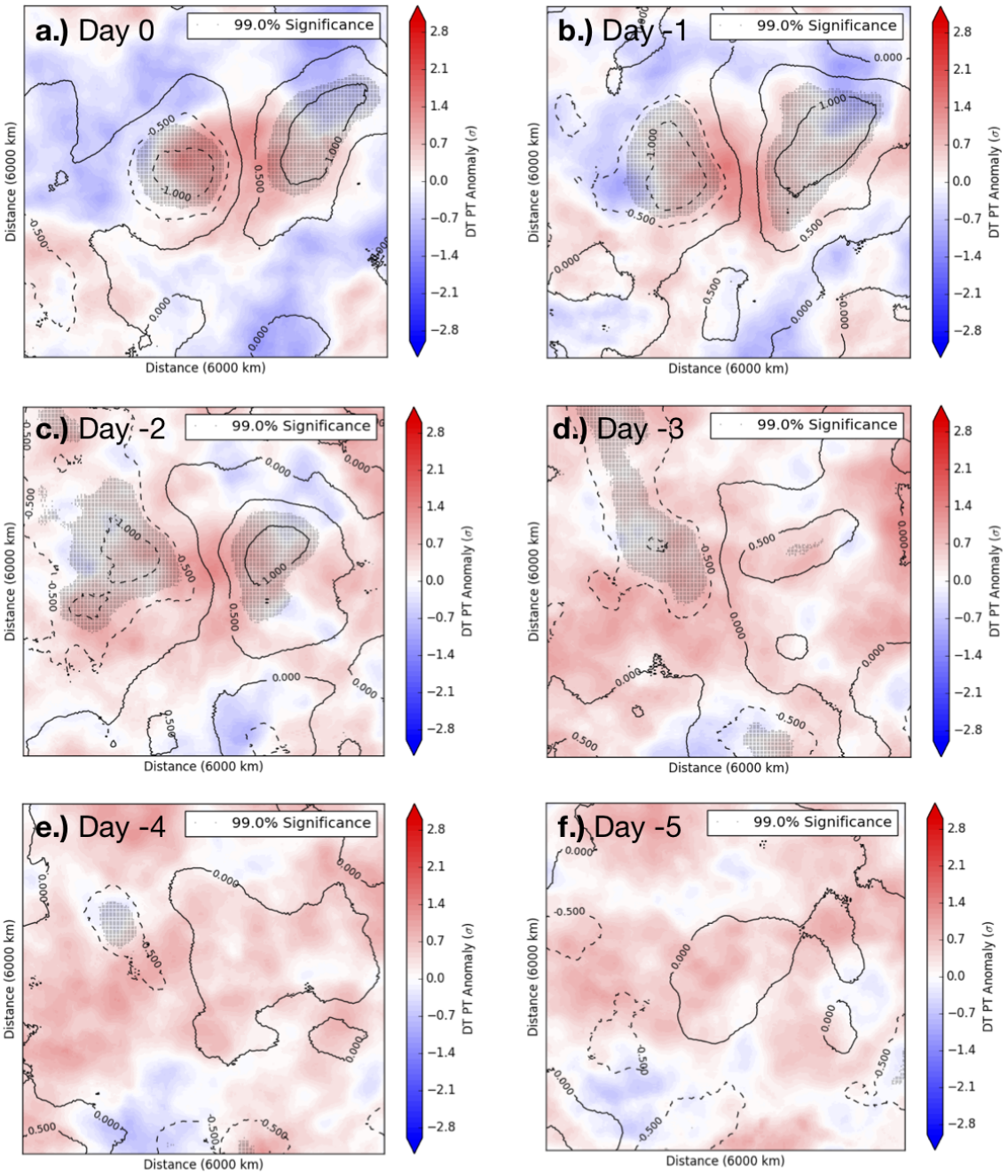

Figure 4.8: Summer, time lagged, composite means of standardized anomalies of mslp, represented by the black contours, and θ on the 2 PVU surface, represented by the shaded background, centered on the VRILE location. Both fields are shown from -3 to 3 σ with mslp contoured every 0.5σ. Grey stippling indicates statistical significance of the mslp field at the 99% level. Panels (a) - (f) correspond to day 0 to -5 relative to the VRILE.

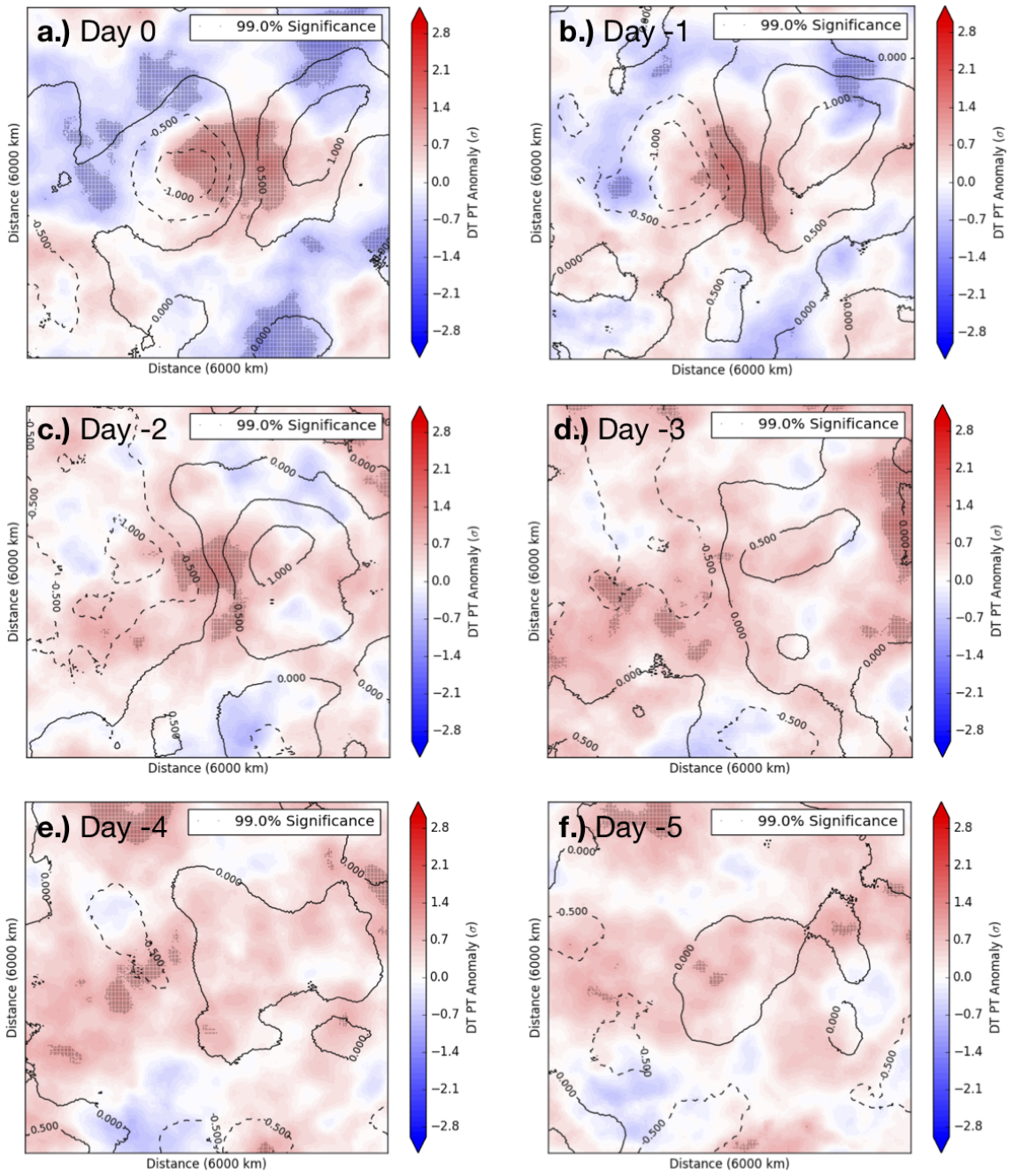

Figure 4.9: Summer, time lagged, composite means of standardized anomalies of mslp, represented by the black contours, and θ on the 2 PVU surface, represented by the shaded background, centered on the VRILE location. Both fields are shown from -3 to 3 σ with mslp contoured every 0.5σ. Grey stippling indicates statistical significance of θ on the 2 PVU surface at the 99% level. Panels (a) - (f) correspond to day 0 to -5 relative to the VRILE.

decreases over time, with the change being more dramatic in the summer than winter. The dipole signal is consistently present in the winter but in the summer is indistinguishable from the background state by the second day.

Figures 4.12 and 4.13 are time lagged composites centered on the θ minima for winter and summer months with panels (a) - (f) corresponding to days 0 to -5 days before the VRILE. In both seasons, there is a TPV present and statistically significant at each time step. The TPV in the winter composites has a larger radius than in the summer. One of the features we observe in Figure 4.5 was a dipole feature on the dynamic tropopause. The corresponding positive θ anomaly remains coherent in the winter until the day 5 (Figure 4.12.f). In the summer, while there remains statistically significant positive θ anomalies in the composite means, it looses the distinct dipole feature around the third day before the VRILE (Figure 4.13.d).

A noteable feature in all of the composites centered on the mslp or θ minima (Figures 4.4, 4.5, 4.10, 4.11, 4.12, and 4.13) is the separation between the TPV and surface cyclone centers. A fully mature surface cyclone would be vertically stacked with the upper level, cyclonic TPV (Hoskins et al. 1985). The tilt between the surface and upper level cyclones suggests that the surface cyclone is strengthening.

4.2.2 Surface Cyclone and TPV Developments in Composite Means

We use the data presented in Section 4.2.1 to examine how the analyzed surface cyclone and TPV evolve in time. Features of interest are the tilt between the TPV and surface cyclone, the surface cyclone's distance from the VRILE location, and the strength of both the surface cyclone and TPV.

The horizontal distance between the centers of the TPV and surface cyclone are shown in Figure 4.14. Figure 4.14.a is for the winter composites and 4.14.b is for summer. In both panels, the blue curve represents the distance between the two centers in the mslp centered

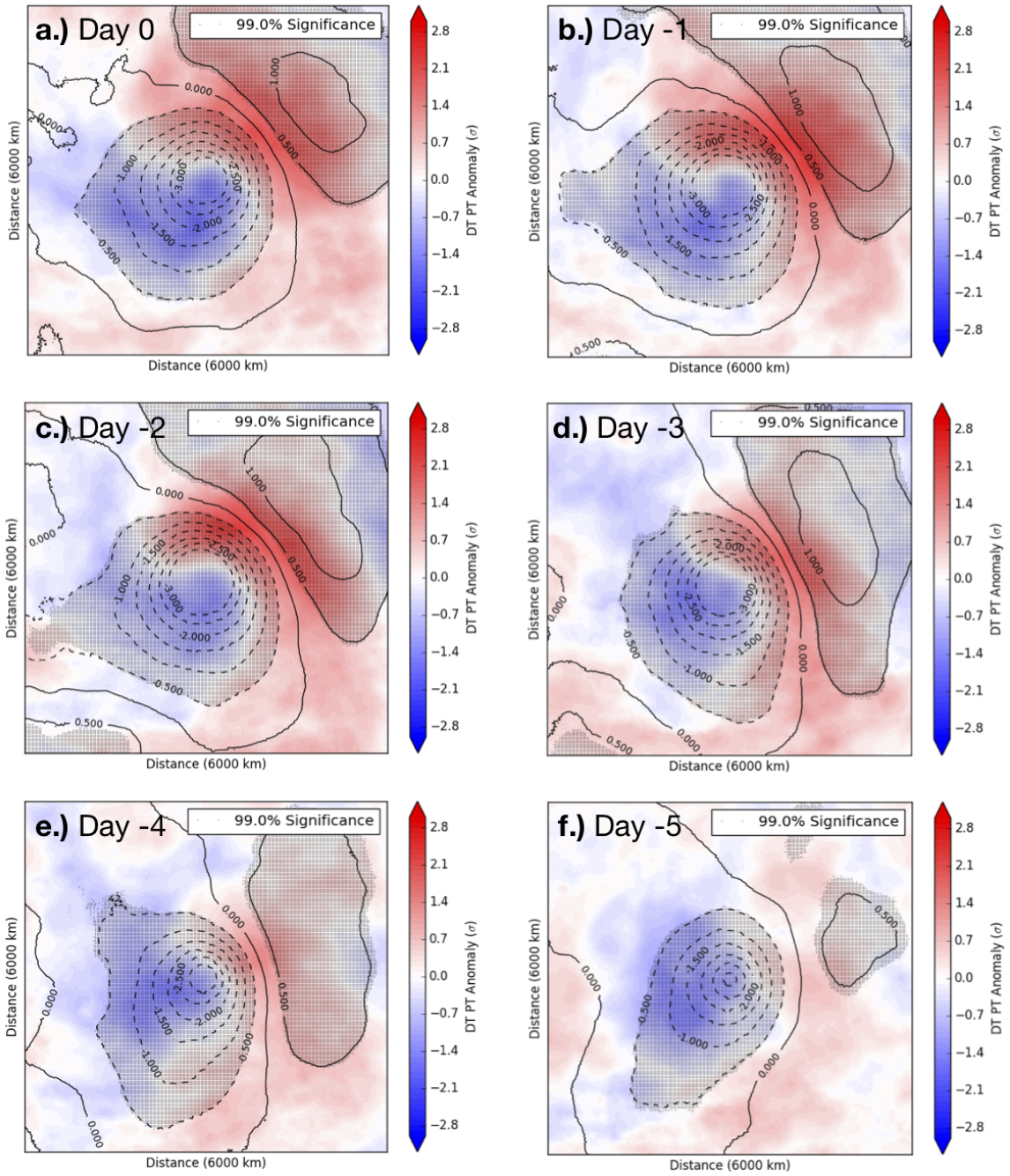

Figure 4.10: Winter, time lagged, composite means of standardized anomalies of mslp, represented by the black contours, and θ on the 2 PVU surface, represented by the shaded background, centered on the closest mslp minima to the VRILE location. Both fields are shown from -3 to 3 σ with mslp contoured every 0.5σ. Grey stippling indicates statistical significance of the mslp field at the 99% level. Panels (a) - (f) correspond to day 0 to -5 relative to the VRILE.

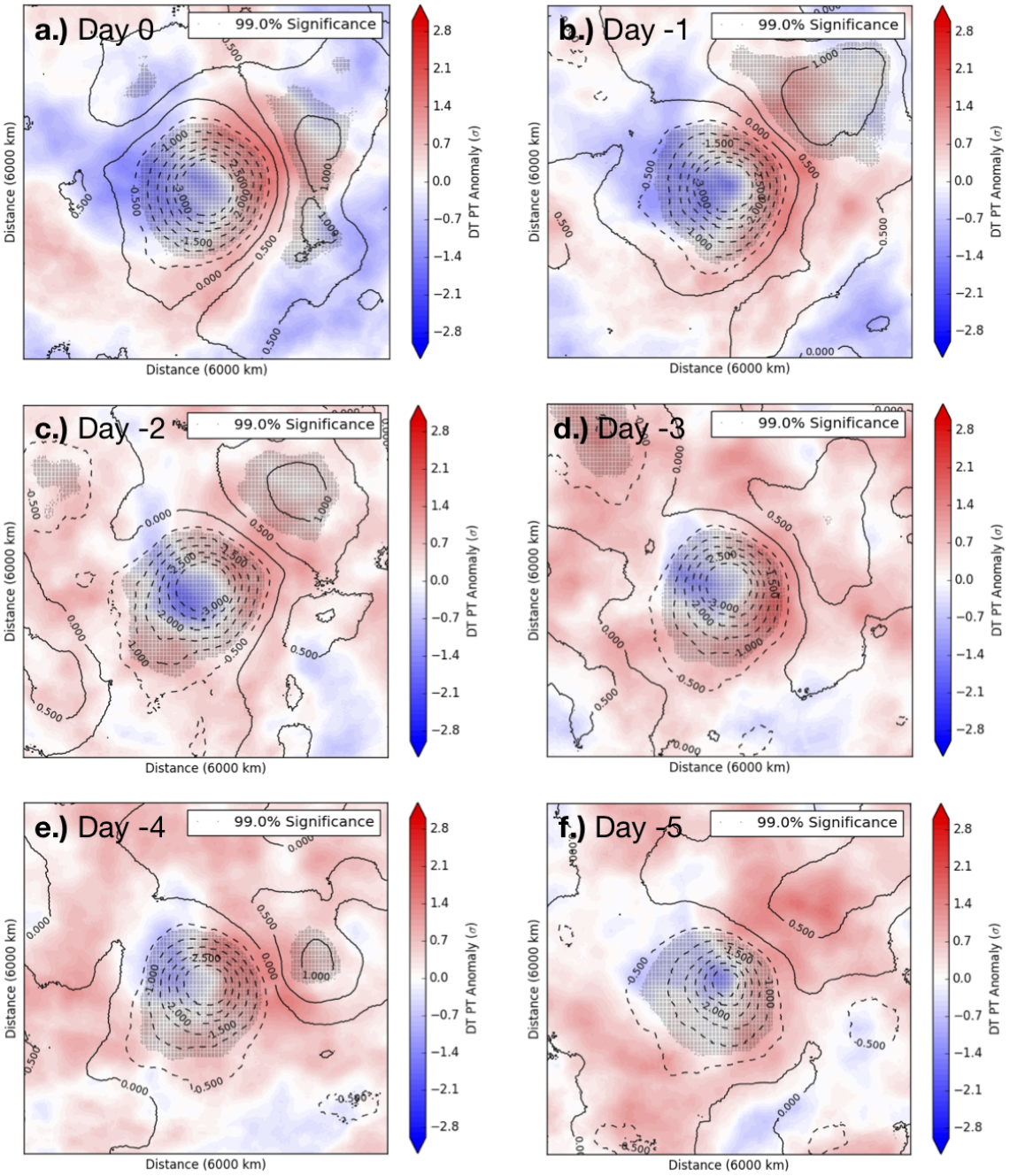

Figure 4.11: Summer, time lagged, composite means of standardized anomalies of mslp, represented by the black contours, and θ on the 2 PVU surface, represented by the shaded background, centered on the closest mslp minima to the VRILE location. Both fields are shown from -3 to 3 σ with mslp contoured every 0.5σ. Grey stippling indicates statistical significance of the mslp field at the 99% level. Panels (a) - (f) correspond to day 0 to -5 relative to the VRILE.

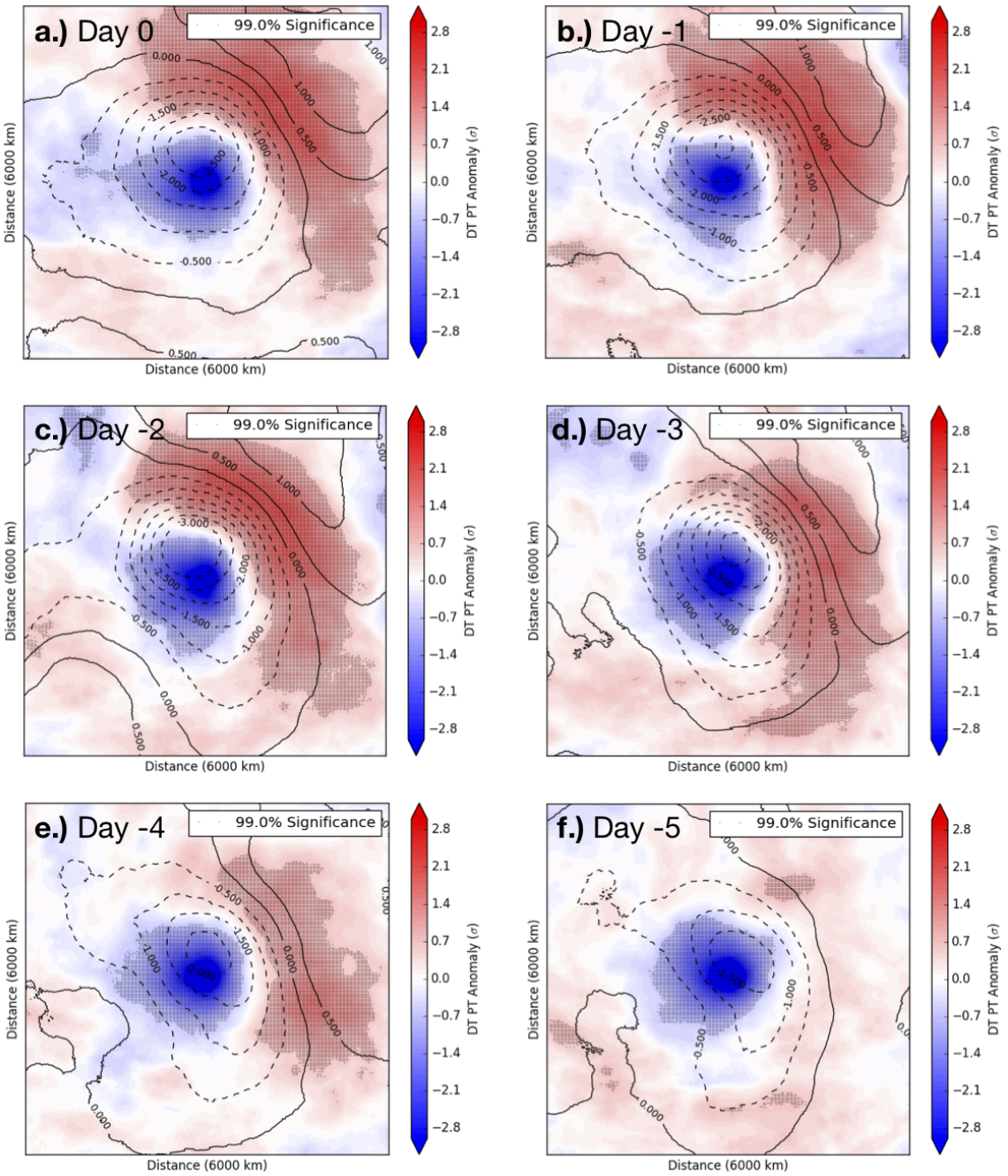

Figure 4.12: Winter, time lagged, composite means of standardized anomalies of mslp, represented by the black contours, and θ on the 2 PVU surface, represented by the shaded background, centered on the closest θ minima on the 2 PVU surface to the VRILE location. Both fields are shown from -3 to 3 σ with mslp contoured every 0.5σ. Grey stippling indicates statistical significance of θ on the 2 PVU surface at the 99% level. Panels (a) - (f) correspond to day 0 to -5 relative to the VRILE.

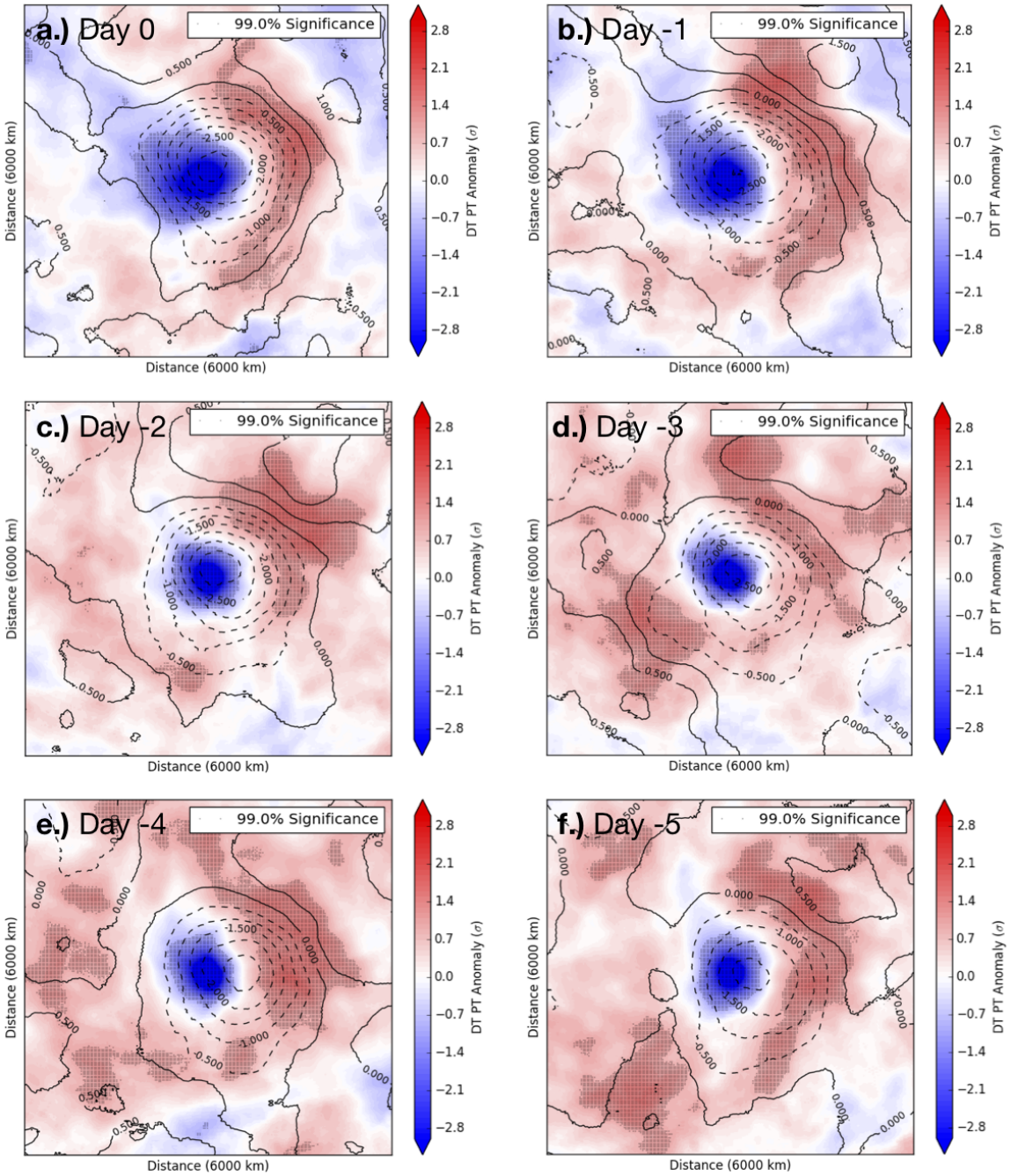

Figure 4.13: Summer, time lagged, composite means of standardized anomalies of mslp, represented by the black contours, and θ on the 2 PVU surface, represented by the shaded background, centered on the closest θ minima on the 2 PVU surface to the VRILE location. Both fields are shown from -3 to 3 σ with mslp contoured every 0.5σ. Grey stippling indicates statistical significance of θ on the 2 PVU surface at the 99% level. Panels (a) - (f) correspond to day 0 to -5 relative to the VRILE.

composites (Figure 4.10 for winter and Figure 4.11 for summer) and the orange curve is for the TPV centered data (Figure 4.12 for winter and Figure 4.13 for summer).

In the winter, the TPV and mslp centered composite data do not agree in terms of the surface cyclone and TPV tilt development in time. When using the TPV centered composite data, the cyclone and TPV get persistently further apart but there is no pattern to their separation in the mslp centered data (Figure 4.14.a). However, in the summer both datasets show the same general trend with the surface cyclone and TPV getting progressively closer together until the day before the VRILE (Figure 4.14.b). This indicates that the surface cyclone is in its mature stage the day before the VRILE. On the day of the VRILE, there is a large discrepancy between the two datasets. In both, the surface cyclone and TPV are further away from each other than the day before but in the mslp centered data the distance jumps to over 1000 km away compared to being approximately vertically aligned the day before. There is no clear reason for this large change to occur. Additionally, while they surface cyclone and TPV are also further apart on the day of the VRILE than the day before in the TPV centered data, the change is much less.

The horizontal distance between the VRILE and the mslp minimum is plotted in Figure 4.15, with summer values plotted in blue and winter in orange. The cyclone's distance from the VRILE location only varies by approximately 100 km over the five day period (Figure 4.15). This may be a product of how the composite mean is calculated, re-centering on the closest, minimum mslp anomaly at each time step.

The strength of the surface cyclone is plotted in Figure 4.16, with winter values in 4.16.a and summer in 4.16.b. As in Figure 4.14 the blue curve represents data from the mslp centered composites (Figure 4.10 for winter and 4.11 for summer) and the orange curve represents data from the TPV centered ones (Figure 4.12 for winter and 4.13 for summer).

In the winter, the surface cyclone reaches its minimum mslp two days before the VRILE (Figure 4.16.a). The magnitudes are different between the TPV and mslp centered data,

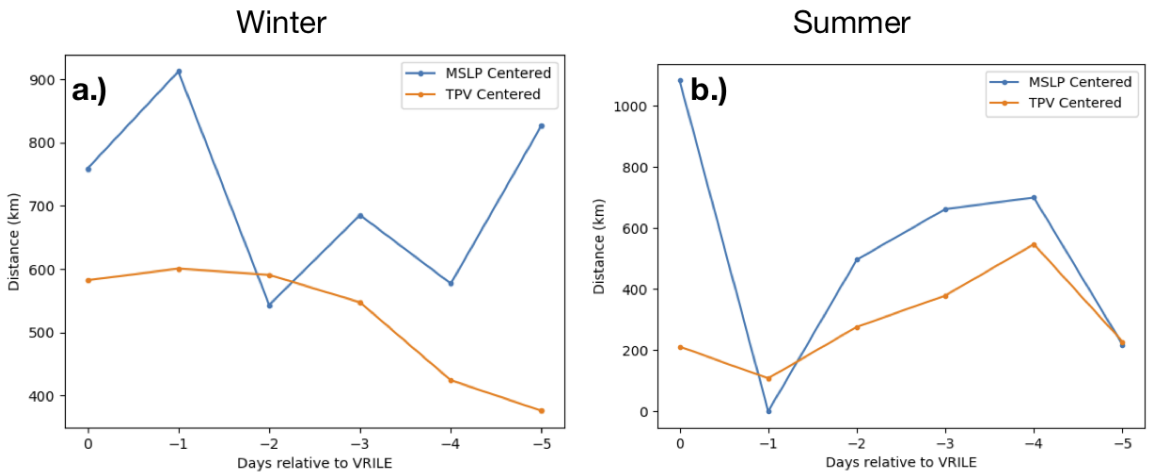

Figure 4.14: The distance between the TPV and surface cyclone centers in the winter (a) and summer (b) composite means. Blue curves represent data from the mslp centered composites and orange curves represent data from TPV centered composites.

with the mslp centered data indicating, as expected, a stronger signal. This result is consistent with the increase in the strength of the pressure signal in the winter, VRILE centered composite data being greatest two days before the VRILE (Figure 4.6). As discussed in conjunction with that figure, the data may be capturing some form of dynamic preconditioning of the sea ice necessary for winter VRILEs to occur. The surface cyclone reaching its maximum strength two days before the VRILE supports that analysis. In the summer, the strength of the cyclone generally increases with time in both datasets (Figure 4.16.b).

The final feature investigated is the strength of the TPV, plotted in Figure 4.17. Again, 4.17.a is for winter months with the blue curve representing data from the mslp centered composites (Figure 4.10) and the orange curve is taken from the TPV centered ones (Figure 4.12) while 4.17.b is for the summer months with the curves also corresponding to mslp centered (Figure 4.11) and TPV centered (Figure 4.13) data. There is no discernible trend in the strength of the TPV in either winter or summer (Figure 4.17).

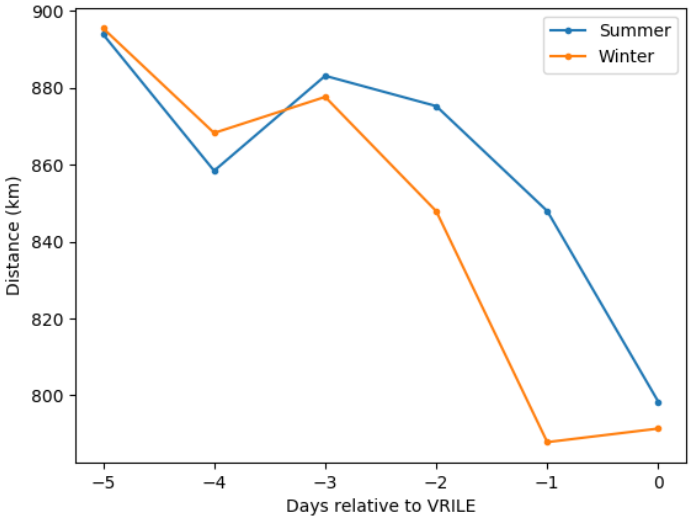

Figure 4.15: Distance between the VRILE location and the surface cyclone from mslp centered composites. The blue curve is for summer values and the orange curve is for winter.

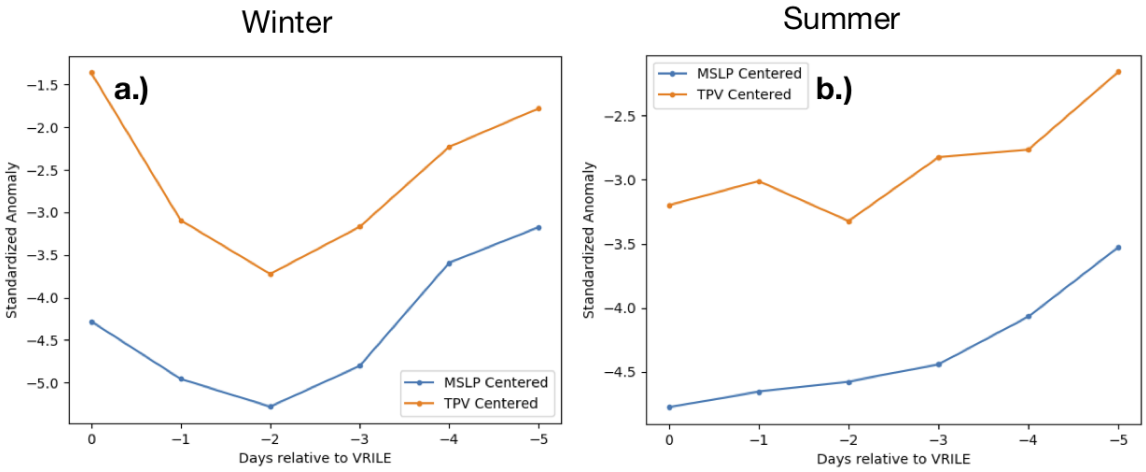

Figure 4.16: Minimum mslp from the time lagged composite mean data. Data for the winter are presented in panel (a) and the summer in panel (b). Blue curves represent data from the mslp centered composites and orange curves represent data from TPV centered composites.

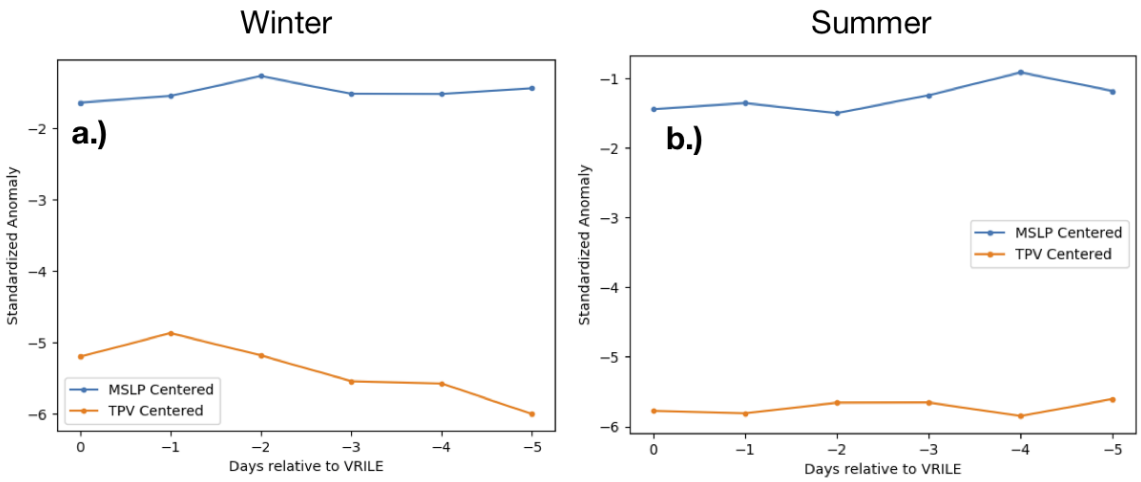

Figure 4.17: Plots of the min θ from the time lagged composite mean data. Data for the winter are presented in panel (a) and the summer in panel (b). Blue curves represent data from the mslp centered composites and orange curves represent data from TPV centered composites.

4.3 Connecting Cyclone Tracks and VRILEs

The first half of this chapter shows a relationship between VRILEs, cyclones, and TPVs through composite means. Here we investigate that association between cyclones and VRILEs from a different perspective by using cyclone track lists. Matching VRILEs to individual cyclones in this manner is independent from the analyses in Section 4.2.2, adding confidence to our hypothesis that surface cyclones tend to proceed VRILEs. This section is divided into three parts. First we composite ice loss objects and cyclone tracks, then we match individual VRILEs to the cyclone tracks, and lastly we discuss the results of these investigative tools.

4.3.1 Compositing VRILEs

In order to match individual cyclones with specific VRILEs, we need to have a sense of how close a cyclone needs to be to the VRILE in order to affect the sea ice. We got a

rough idea in Section 4.2.2 by considering the average distance between the VRILE and local mslp minima, finding that the local minima in mslp tends to be between 800 and 900 km away from the point within the sea ice concentration loss object that experienced the greatest negative change (Figure 4.15).

The shading in Figure 4.18 represents the sum of the ice loss objects used to identify VRILE locations described in Section 2.3. Recall that the ice loss objects are stored as masks, with each grid point give a value of one if it lies within the object and a zero otherwise. Each loss object is centered on the point that experienced the greatest sea ice loss. Therefore the center point of Figures 4.18.a and 4.18.b is equal to the total number of VRILEs for that season, 141 for the winter events (Figure 4.18.a) and 76 for the summer (Figure 4.18.b). Taking the sum in this manner presents an image of the general shape and size of each season's VRILEs.

Plotted on top of the ice loss objects are cyclone locations from NCEP/NCAR reanalysis. In order to be included, the cyclone location had to be less than 2000 km from any point within the ice loss object between 0 and -5 days of a particular VRILE. The points are color coded according to their minimum distance from the ice loss object. Orange indicates a minimum distance of < 500 km, magenta indicates between 500 and 1000 km, red between 1000 and 1500 km, and black points are between 1500 and 2000 km away from the ice loss object.

The composite image of the winter VRILEs has less variability in size and shape than its summer counter part. Winter VRILEs appear smaller and more circular, evidenced by the tight, dark blue center of the figure (Figure 4.18.a). In the summer however, the edges are less defined (Figure 4.18.b). Similarly, the distribution of cyclone locations are more tightly grouped and have a more distinct gradient in the distance from the VRILE in the winter than in the summer. These differences are consistent with winter VRILEs being less variable in size.

The main purpose in creating Figure 4.18 is to gain insight into how close a cyclone has to be to the VRILE in order to affect it. Ideally, we would be able to have a criteria that included every cyclone associated with a VRILE and excluded all others. However that idea is not practical given the limitations of our data. In creating a dataset of cyclone associated with VRILEs, we would rather have false negatives than false positives. That is, we would rather exclude a cyclone from the dataset that actually is associated with a cyclone than include one that is not. Qualitatively looking at Figure 4.18, the 500 km cutoff seems too restrictive and the 2000 km cutoff too lenient. Both the 1000 and 1500 km cutoff distances appear to strike a balance.

4.3.2 Cyclone Matching

Both 1500 km and 1000 km are used as cutoff distance for whether a cyclone is associated with a VRILE or not. We then use both NCEP/NCAR and ERA-I reanalysis cyclone track lists and identify cyclones that passed within the cutoff distance no more than five days before the VRILE. In Table 4.1 the total number of cyclones identified in each season is presented. Recall that the ERA-I track list is for 1984 - 2016 while the NCEP/NCAR list is for 1979 - 2016. Therefore there are fewer ERA-I cyclones identified than NCEP/NCAR in every category.

More VRILEs occur in the winter than the summer, 141 versus 76 for the Butterworth filter definition. Therefore it is somewhat unsurprising that from NCEP/NCAR, more cyclones are identified in the winter than the summer. However, that is not the case with the ERA-I cyclones. Table 4.2 provides some additional information on this inconsistency. There are noticeably more winter VRILEs without an associated cyclone than for summer VRILEs. This is especially true with the 1500 km threshold is used.

For summer VRILEs, the number of VRILEs without an associated cyclone are effectively identical in both track lists. The same cannot be said for winter VRILEs. Note that for the ERA-I list, only VRILEs that occurred in 1984 or later are counted because the

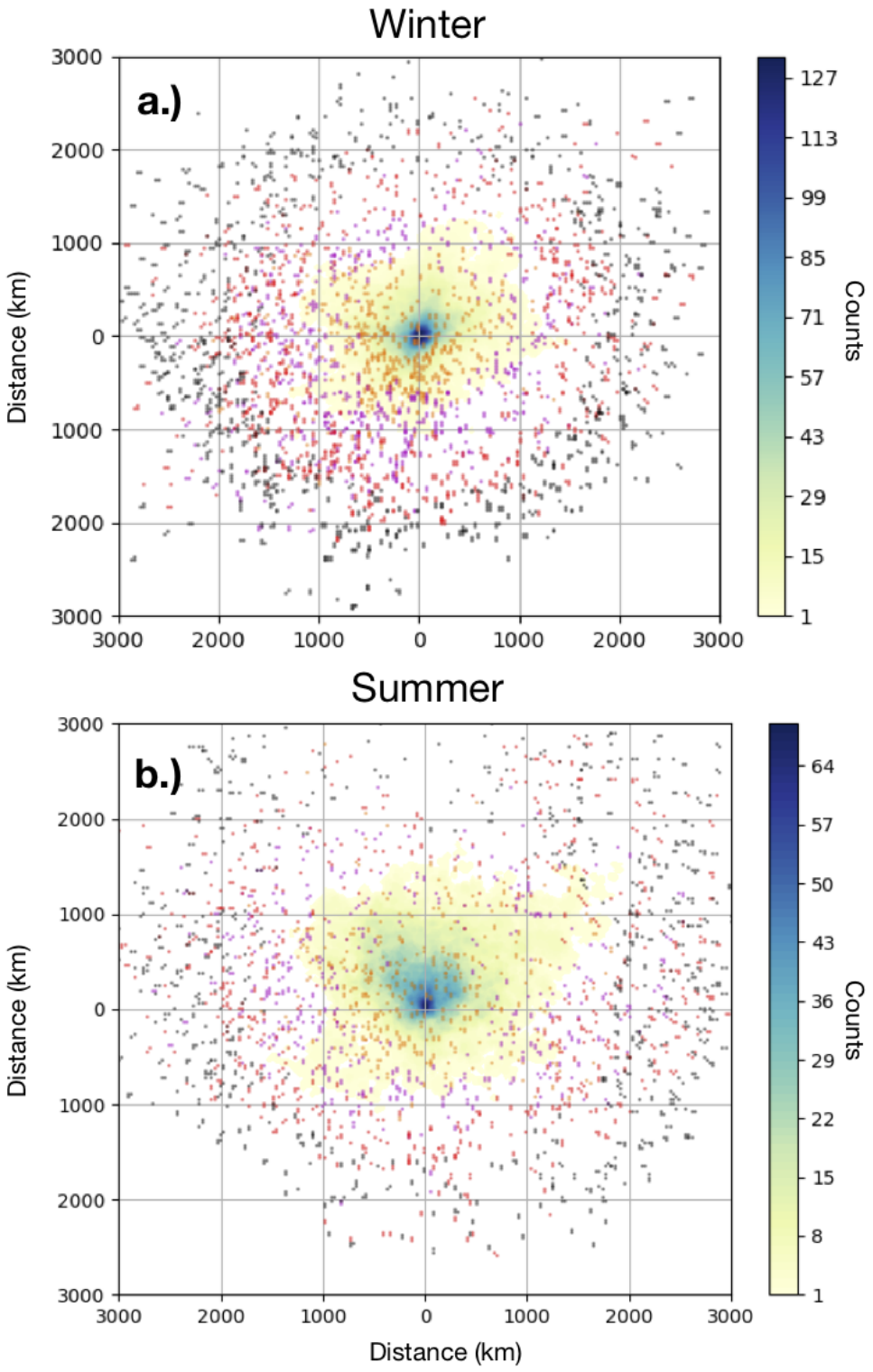

Figure 4.18: Composite of VRILE objects for winter (a) and summer (b) events. Points indicate the location of a cyclone associated with a VRILE. The color of the points indicates its distance from the VRILE. Orange: 0 - 500 km, Magenta: 500 - 1000 km, Red: 1000 - 1500 km, Black: $>$ 1500 km

ERA-I cyclone list does not include tracks before then. Even with fewer VRILEs, there are noticeably more without an associated cyclone from the ERA-I list than NCEP/NCAR.

In order to understand the discrepancies between the number of cyclones associated with winter VRILEs between the reanalysis products, we consider the location of the VRILEs without an associated cyclone (Figure 4.19). Figure 4.19.a shows the locations of winter VRILEs without an associated cyclone from the NCEP/NCAR cyclone list and Figure 4.19.b shows the locations of winter VRILEs without an associated cyclone from the ERA-I cyclone list.

One potential reason that there are so many more winter VRILEs without associated cyclones than summer is that winter VRILEs tend to occur further south. The cyclone track lists being used are specifically for Arctic cyclones, defined as any cyclone that travels north of 60°. There may be cyclones associated with the VRILEs in Figure 4.19 that are not classified as Arctic cyclones and consequently were not included in the cyclone track lists.

While there is much overlap between the locations of VRILEs without an associated cyclone from both track lists, the most obvious difference in the ERA-I list is a cluster of VRILEs south of the Bering Strait (Figure 4.19.b, circled region). The second most noteable difference between the VRILE locations in Figure 4.19 is the cluster of location northeast of Greenland. Differences between which winter VRILEs have an associated cyclone and which do not between the reanalysis datasets may be attributable to differences in the tracking algorithms used. The algorithm used on the NCEP/NCAR data identified maxima in the Laplacian of pressure, $\nabla^2 P$, predicts its location forward in time and uses that predicted location to compare against data from the next time step. The full details of the tracking algorithm used are outlined in Murray and Simmonds (1991), with modifications specified by Simmonds and Murray (1999) and Simmonds et al. (1999). The tracking

Cyclone Tracks	Season	1000 km	1500 km
NCEP/NCAR	Summer	197	297
	Winter	233	358
ERA-I	Summer	179	248
	Winter	141	233

Table 4.1: Number of cyclones identified to pass within 1000 km of the VRILEs no more than five days before the event. Note that the ERA-I is from 1984-2016 while NCEP/NCAR is from 1979-2016.

Cyclone Tracks	Season	1000 km	1500 km
NCEP/NCAR	Summer	7	2
	Winter	37	27
ERA-I	Summer	8	3
	Winter	58	40

Table 4.2: Number of VRILEs without an associated cyclone. Note that the ERA-I is from 1984-2016 while NCEP/NCAR is from 1979-2016.

algorithm used on the ERA-I reanalysis however, tracks mslp minima but allows for a single cyclone to have up to three minima and still be considered a single structure (Hanley and Caballero 2012). This method is designed to capture merging and splitting events.

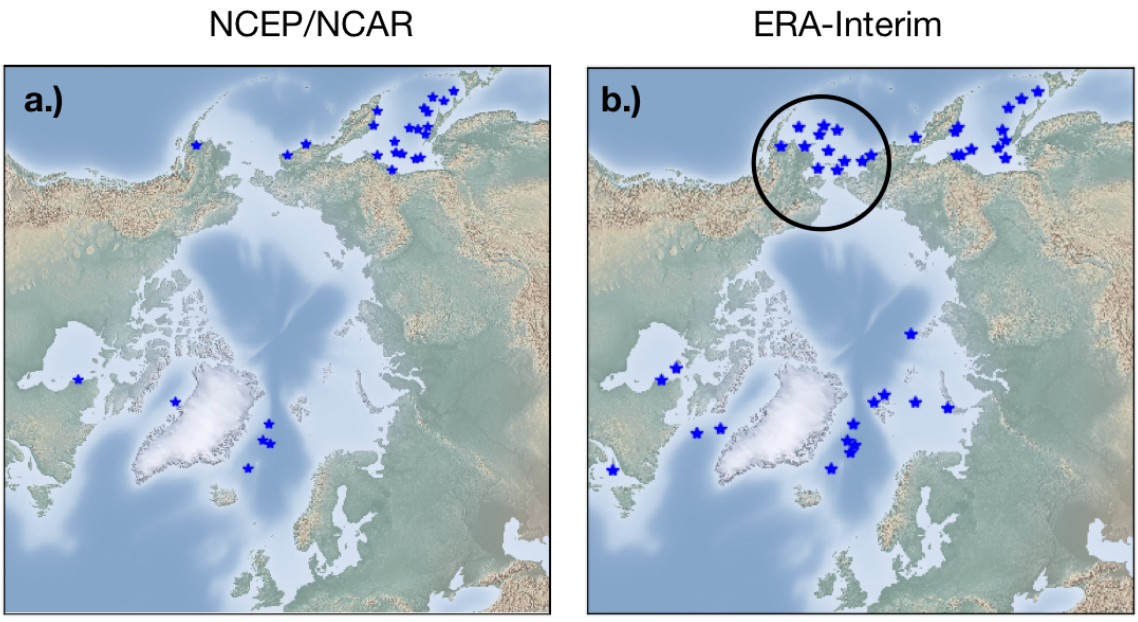

Figure 4.19: Location of winter VRILEs without an associated cyclone. Panel (a) is for the NCEP/NCAR reanalysis cyclone tracks and panel (b) if for the ERA-I track list. The circled area highlights a region of noteable differences between (a) and (b).

Chapter 5

Cyclone Properties

5.1 Probability Density Functions

The cyclone properties we examine are lifetime, minimum mslp, mean speed, and maximum radius. Probability density functions (PDFs) of these properties for cyclones associated with VRILEs and cyclones that are not are presented in Figures 5.1, 5.2, 5.3, and 5.4. For each of those figures, panel (a) refers to winter cyclones and panel (b) summer. The mean values of each PDF as well as the p value of the K-S test is presented in Table 5.1. Table 5.1 also shows the mean values for minimum mslp, mean speed, and maximum radius for cyclones associated with VRILEs restricted to only the five days before the VRILE occurred and p values associated with those limited distriubutions.

Cyclones associated with VRILEs tend to be longer lived and larger than those that are not (Figures 5.1 and 5.4). The strength of the cyclone, determined by its lifetime minimum mslp, is not a significant factor in whether a cyclone precedes a VRILE or not (Figure 5.2). While winter cyclones associated with VRILEs tend to travel slower than other winter cyclones, that relationship is not statistically significant. Summer cyclones associated with VRILEs are significantly faster than those that are not (Figure 5.3).

Some of those properties change when we only consider cyclone data within five days of the VRILE occurring. In both seasons, the maximum radius shrinks and is less than the average for cyclones not associated with VRILEs. The speed increases and is greater than the average for cyclones not associated with VRILEs. The minimum mslp is still not statistically significant and in fact is larger than the overall mean for the cyclone (Table 5.1).

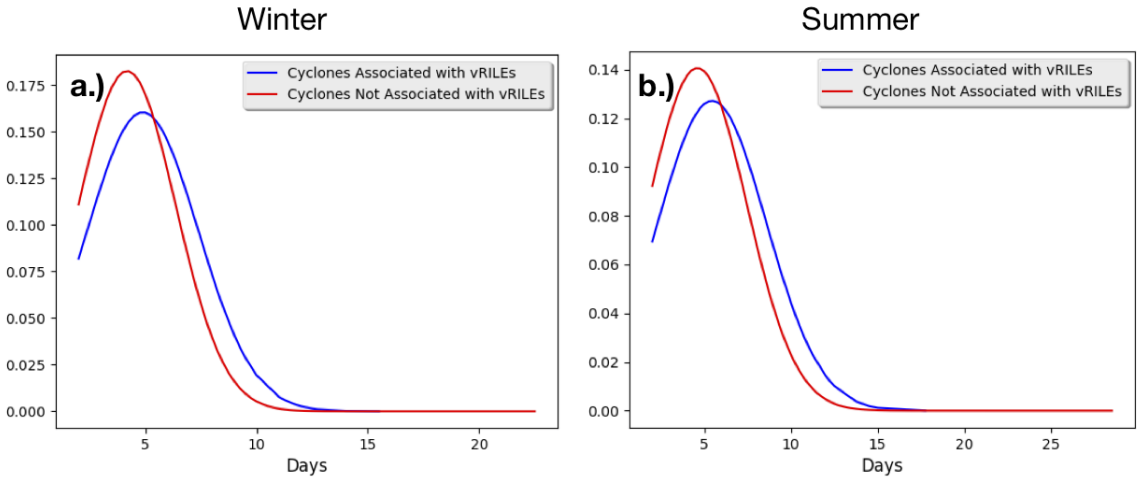

Figure 5.1: Probability density functions of the lifetime, in days, of cyclones associated with VRILEs (blue) and cyclones that are not (red). Panel (a) is for winter cyclones and panel (b) is for summer.

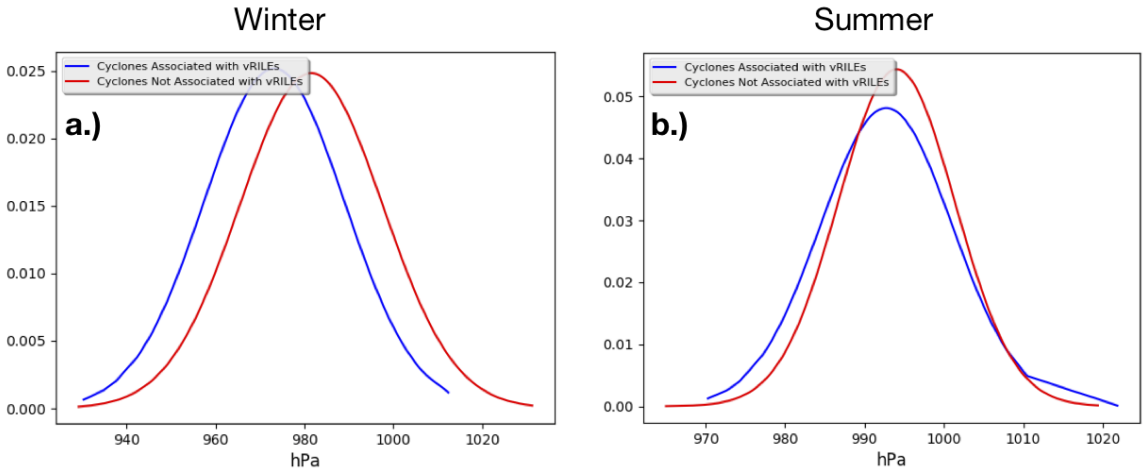

Figure 5.2: Probability density functions of the minimum mslp of the cyclone, in hPa, of cyclones associated with VRILEs (blue) and cyclones that are not (red). Panel (a) is for winter cyclones and panel (b) is for summer.

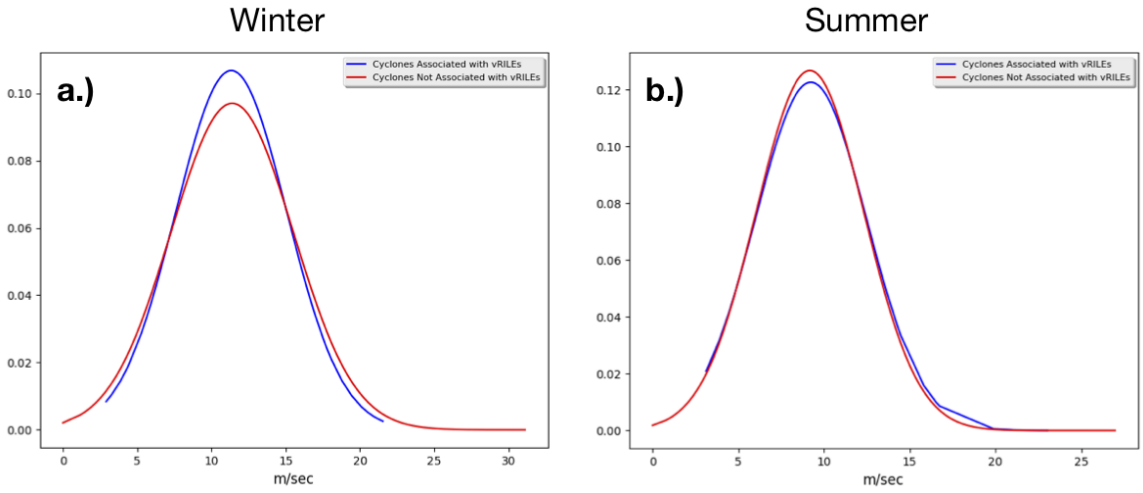

Figure 5.3: Probability density functions of mean speed, in m per sec, of cyclones associated with VRILEs (blue) and cyclones that are not (red). Panel (a) is for winter cyclones and panel (b) is for summer.

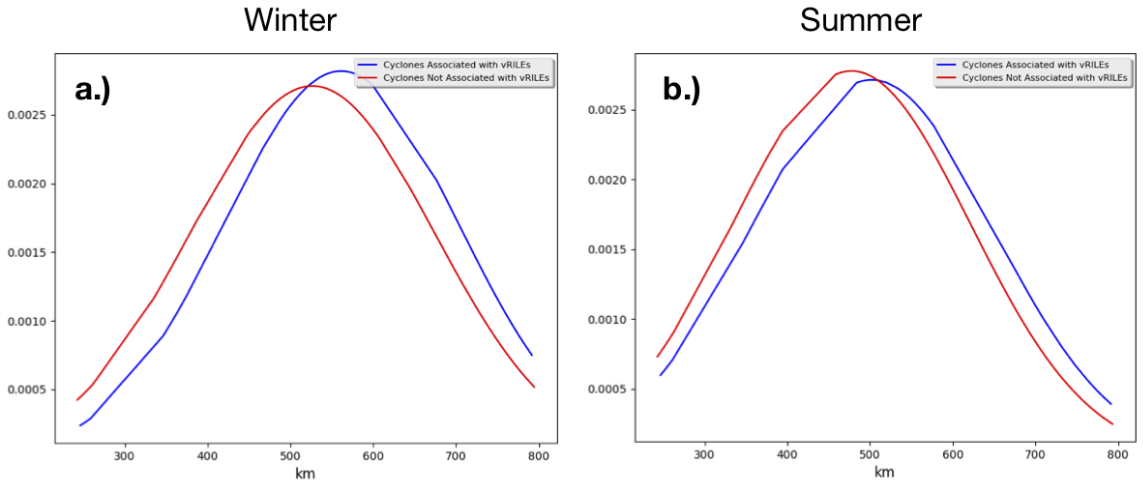

Figure 5.4: Probability density functions of the cyclone's maximum radius, in km, of cyclones associated with VRILEs (blue) and cyclones that are not (red). Panel (a) is for winter cyclones and panel (b) is for summer.

Season		Associated with VRILEs	Not Associated with VRILEs	P Value
Winter	Lifetime (days)	4.89	4.12	0.005
	Minimum MSLP (hPa)	973.22	981.55	0.4
	Maximum Radius (km)	561.32	526.58	< 0.001
	Average Speed (m/sec)	11.33	11.39	0.26
Summer	Lifetime (days)	5.45	4.61	< 0.001
	Minimum MSLP (hPa)	992.75	994.04	0.03
	Maximum Radius (km)	502.16	477.6	< 0.001
	Average Speed (m/sec)	9.24	9.18	< 0.001
		Within 5 Days		
Winter	Minimum MSLP (hPa)	976.86	981.55	0.5
	Maximum Radius (km)	505.24	526.58	< 0.001
	Average Speed (m/sec)	11.7	11.39	0.001
Summer	Minimum MSLP (hPa)	994.87	994.04	0.12
	Maximum Radius (km)	437.75	477.6	0.001
	Average Speed (m/sec)	9.46	9.18	< 0.001

Table 5.1: Mean values of various properties for cyclones in the NCEP/NCAR reanalysis track list that. Cyclones are divided into those that are and are not associated with a VRILE. The last column shows the p value determined by the K-S test. Statistically significant results are shaded in grey.

5.2 Sea Ice Environment

To understand the sea ice environment cyclones associated with VRILEs interact with, we consider the cyclones' distance from the 15% and 95% sea ice concentration contours on the day the VRILE occurred. Figure 5.5 shows the histogram of the distance from the 15% sea ice concentration contour for winter (5.5.a) and summer (5.5.b) cyclones. The histograms of cyclone distance from the 95% contour are shown in Figure 5.6, with distances for winter cyclones in 5.6.a and 5.6.b for summer cyclones.

Summer cyclones associated with VRILEs are, on average, 1800 km from the 15% sea ice concentration contour and 2700 km from the 95%. Distance is calculated as the minimum distance between the cyclone center and the given contour at the time of the VRILE. For the 15% contour, which is the typical value used to denote sea ice extent, the distribution of distances is highly concentrated to the shorter distances (Figure 5.5.b), but is more spread out for the 95% contour (Figure 5.6.b). However, the distributions of the winter cyclone distances have a nearly normal distribution for both sea ice concentration contours with nearly identical mean distances of 5000 km (Figures 5.5 and 5.6.a). These distributions are an indication that summer cyclones associated with VRILEs are along the sea ice edge, which supports our hypothesis that cyclones interacting with thin ice are more likely to results in VRILEs. However the same trend is not observed in the winter cyclones.

There is insufficient evidence to make any firm conclusions regarding the sea ice conditions required for a VRILE to occur. Results show that the winter cyclones tend to have larger radii than summer cyclones and consequently the location of the cyclone's center may be less important. The difference in these distributions could also be a result of differences in sea ice preconditioning. If, in the summer, thermodynamic processes are the predominant means of preconditioning then cyclones are more likely to interact with already thin ice. On the other hand, if in the winter the cyclone itself is dynamically conditioning the ice, then its distance from the ice edge on the day the VRILE occurs may be less important than its location in the days before the VRILE. Additionally there are many

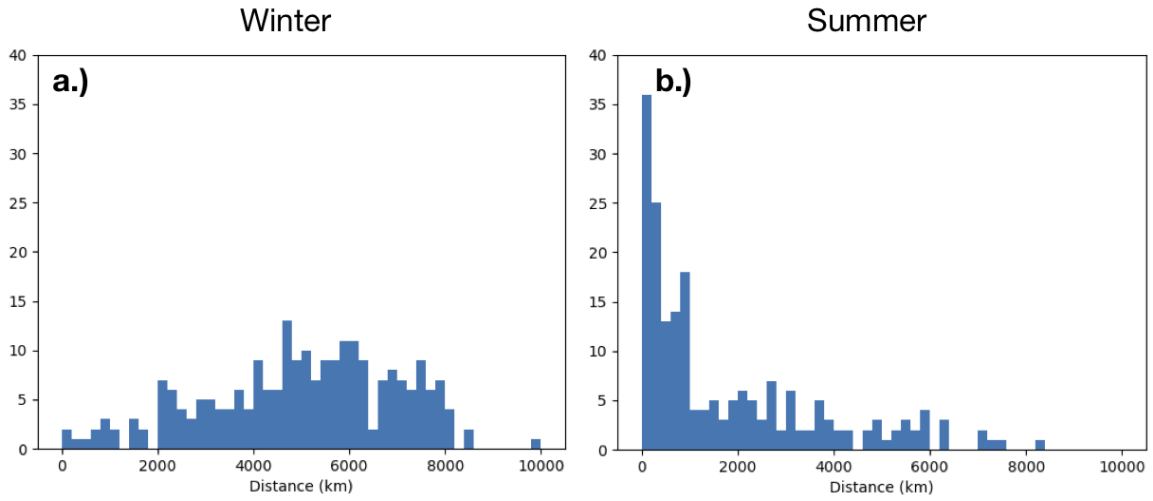

Figure 5.5: Histograms showing the distance from the cyclone center and the 15% sea ice concentration contour on the day the VRILE occurred for winter (a) and summer (b) cyclones.

winter VRILEs that do not match to a cyclone. If the reason for that was because cyclones associated with those VRILEs never traveled north of 60°, then including those cyclones in these distributions may change them.

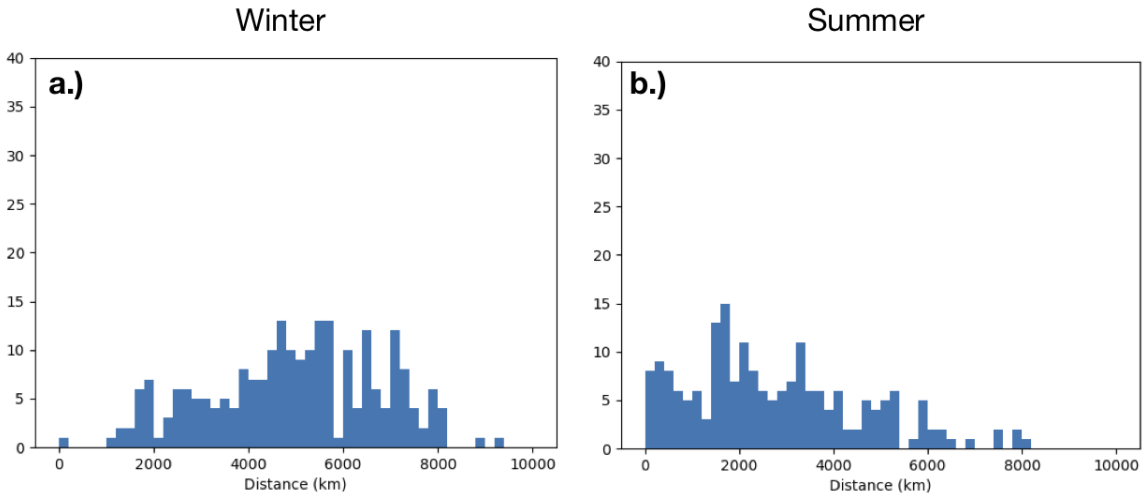

Figure 5.6: Histograms showing the distance from the cyclone center and the 95% sea ice concentration contour on the day the VRILE occurred for winter (a) and summer (b) cyclones.

Chapter 6

Conclusions

The goals of this thesis were twofold: 1.) to establish that VRILEs tend to be proceeded by a cyclone with an associated TPV; and 2.) to quantify what about the cyclone and sea ice environment made the VRILE possible. We hypothesized that long lived cyclones over thin ice, using sea ice concentration as a proxy for thickness, have the greatest potential to affect sea ice loss.

The first step was to establish where and when VRILEs occurred. We used two different filtering methods on the daily, sea ice extent changes, either removing the daily, climatological mean value or applying a Butterworth filter to remove changes to sea ice extent with a period greater than 18 days. A third list of VRILEs was created by combining the two lists of VRILEs generated by both filtering methods without overlap. The location of the VRILEs were then used to create composites of standardized anomalies in mslp and θ on the 2 PVU surface centered on the VRILE itself, the closes minima in mslp to the VRILE, and the closest θ minima on the 2 PVU surface. Composites were made on the day of the VRILE for all three VRILE location lists and daily composites going back to five days before the VRILE for the Butterworth filter definition. VRILE locations were also compared to cyclone locations in track lists derived from NCEP/NCAR and ERA-I reanalysis. This was done as an independent means of verifying cyclones proceeding VRILEs.

Matching individual cyclones from reanalysis datasets resulted in two populations of cyclones: those that were associated with VRILEs and those that were not. We then compared various cyclone properties between these two populations to determine which were statistically significant. To test the part of our hypothesis regarding the necessity of thin ice, we compared the distance of the cyclones associated with VRILEs from the sea ice

edge, represented by 15% sea ice concentration, and the center of the ice pack, taken to be 95% sea ice concentration.

A surface cyclone paired withe a TPV is clearly present in the composite means for any definition of VRILE in both winter and summer (Figures 4.4 and 4.5). In the VRILE centered composite means, there was a clear, strong pressure gradient across the VRILE again regardless of season or VRILE definition (Figure 4.3). One of the more interesting results from the composite means was the differences between how that pressure gradient differed in time between summer and winter composites (Figures 4.6 and 4.8). In the winter, the mslp change across the VRILE is strongest two days before the VRILE occurred (Figure 4.6). Additionally, in the mslp and TPV centered composites the winter mslp minima is also strongest two days before the VRILE (Figure 4.16). In the summer, both the pressure change across the VRILE and the strength of the composite, surface cyclone were strongest the day the VRILE occurred (Figures 4.8 and 4.11). However, in the summer the surface cyclone is at its most mature, nearly vertically aligned with the TPV, one day before the VRILE (Figure 4.14). These differences may point to different preconditioning mechanisms necessary for VRILEs in winter versus summer.

A specific cyclone track can be matched to a summer VRILE 97% of the time. While there were more VRILEs in the winter without an associated cyclone, 80% of VRILEs could be paired with a specific track. Many of the winter VRILEs without an associated cyclone were located fairly far south (Figure 4.19). These VRILEs were potentially associated with a surface cyclone that was too far south to be counted in the cyclone track lists as an Arctic cyclone.

By comparing probability density function of cyclone lifetime, strength, maximum radius, and average speed, we have shown that the cyclones preceding VRILEs tend to be longer lived than cyclones overall (Figures 5.1, 5.2, 5.3, and 5.4). We have also shown that strength alone is not a significant factor in whether or not a cyclone will result in a VRILE.

While overall cyclones associated with VRILEs tend to be larger than average, when we restrict ourselves to the five days preceding the VRILE, the radius tends to be smaller. These cyclones also tend to be faster than the general population of Arctic cyclones.

We have shown that VRILEs tend to occur on or near the ice edge, where the ice is typically thinnest. However, we were unable to precisely characterize the sea ice environment within which cyclones associated with VRILEs interact. Cyclones associated with summer VRILEs tend to be closer to the sea ice edge than the central ice pack and their distribution of distances from the sea ice edge was strongly skewed towards shorter distances. However cyclones associated with winter VRILEs were not skewed towards the sea ice edge and were on average equidistant from the sea ice edge and the 95% sea ice concentration contour.

Prior studies addressing VRILEs focused on single events, such as the ice loss caused by the Great Arctic Cyclone in 2012 (Simmonds and Rudeva 2012). Here we have expanded upon those individual studies and established a general relationship between VRILEs and surface cyclones.

One avenue of future research is to expand the surface cyclone tracks used so that they are not restricted to Arctic cyclones. Additionally, pairing tracks of TPVs with surface cyclone tracks would potentially allow us to characterize properties of the TPVs associated with VRILEs and the coupled TPV and surface cyclone systems. A coupled sea ice, ocean, and atmospheric model could be applied to this type of system to better understand the seasonal differences in sea ice preconditioning as well as the importance of sea ice thickness to VRILE occurrences.

Bibliography

Årthun, M., T. Eldevik, L. Smedsrud, Ø. Skagseth, and R. Ingvaldsen, 2012: Quantifying the influence of atlantic heat on barents sea ice variability and retreat. *Journal of Climate*, **25 (13)**, 4736–4743.

Asplin, M. G., R. Galley, D. G. Barber, and S. Prinsenberg, 2012: Fracture of summer perennial sea ice by ocean swell as a result of arctic storms. *Journal of Geophysical Research: Oceans*, **117 (C6)**.

Asplin, M. G., R. Scharien, B. Else, S. Howell, D. G. Barber, T. Papakyriakou, and S. Prinsenberg, 2014: Implications of fractured arctic perennial ice cover on thermodynamic and dynamic sea ice processes. *Journal of Geophysical Research: Oceans*, **119 (4)**, 2327–2343.

Barnhart, K. R., C. R. Miller, I. Overeem, and J. E. Kay, 2016: Mapping the future expansion of arctic open water. *Nature Climate Change*, **6 (3)**, 280.

Blunden, J., and D. S. Arndt, 2012: State of the climate in 2011. *Bulletin of the American Meteorological Society*, **93 (7)**, S1–S282.

Boé, J., A. Hall, and X. Qu, 2009: September sea-ice cover in the arctic ocean projected to vanish by 2100. *Nature Geoscience*, **2 (5)**, 341.

Bryson, R. A., 1965: Air masses, streamlines, and the boreal forest. *Geogr. Bull*, **8**, 228–269.

Cavallo, S. M., and G. J. Hakim, 2009: Potential vorticity diagnosis of a tropopause polar cyclone. *Monthly Weather Review*, **137 (4)**, 1358–1371.

Cavallo, S. M., and G. J. Hakim, 2010: Composite structure of tropopause polar cyclones. *Monthly Weather Review*, **138 (10)**, 3840–3857.

Cavallo, S. M., W. C. Skamarock, and N. Szapiro, 2016: Extended range predictions over the arctic with the model for the prediction across scales (mpas). *DRI meeting for seasonal prediction*, Monterey, CA, Naval Research Labratory.

Collins III, C. O., W. E. Rogers, A. Marchenko, and A. V. Babanin, 2015: In situ measurements of an energetic wave event in the arctic marginal ice zone. *Geophysical Research Letters*, **42 (6)**, 1863–1870.

Comiso, J. C., 2012: Large decadal decline of the arctic multiyear ice cover. *Journal of Climate*, **25 (4)**, 1176–1193.

Crawford, A. D., and M. C. Serreze, 2016: Does the summer arctic frontal zone influence arctic ocean cyclone activity? *Journal of Climate*, **29 (13)**, 4977–4993.

Curry, J., J. Schramm, and E. Ebert, 1993: Impact of clouds on the surface radiation balance of the arctic ocean. *Meteorology and Atmospheric Physics*, **51 (3-4)**, 197–217.

Day, J. J., and K. I. Hodges, 2018: Growing land-sea temperature contrast and the intensification of arctic cyclones. *Geophysical Research Letters*, **45 (8)**, 3673–3681.

Day, J. J., M. M. Holland, and K. I. Hodges, 2018: Seasonal differences in the response of arctic cyclones to climate change in cesm1. *Climate Dynamics*, **50 (9)**, 3885–3903.

Dee, D. P., and Coauthors, 2011: The era-interim reanalysis: configuration and performance of the data assimilation system. *Quarterly Journal of the Royal Meteorological Society*, **137 (656)**, 553–597, doi:10.1002/qj.828, URL https://rmets.onlinelibrary.wiley.com/doi/abs/10.1002/qj.828, https://rmets.onlinelibrary.wiley.com/doi/pdf/10.1002/qj.828.

Dobrynin, M., J. Murawsky, and S. Yang, 2012: Evolution of the global wind wave climate in cmip5 experiments. *Geophysical Research Letters*, **39 (18)**.

Durkalec, A., C. Furgal, M. W. Skinner, and T. Sheldon, 2015: Climate change influences on environment as a determinant of indigenous health: Relationships to place, sea ice, and health in an inuit community. *Social science & medicine*, **136**, 17–26.

Dzerdzeevskii, B., 1945: Tsirkuliatsionnye skhemy v troposfere tsentral'noi arktiki. *Izdatel'svo Akad. Nauk*.

Eady, E. T., 1949: Long waves and cyclone waves. *Tellus*, **1 (3)**, 33–52.

Eicken, H., A. L. Lovecraft, and M. L. Druckenmiller, 2009: Sea-ice system services: A framework to help identify and meet information needs relevant for arctic observing networks. *ARCTIC*, **62 (2)**, 119–136.

Eliassen, A., and E. Kleinschmidt, 1957: Handbuch der physik. vol. 48. Springer-Verlag.

Farrell, B., 1985: Transient growth of damped baroclinic waves. *Journal of the atmospheric sciences*, **42 (24)**, 2718–2727.

Fetterer, K. K. W. M., F., and M. Savoie, 2002: Sea ice index.

Fetterer, K. K. W. N. M. M. S., F., and A. K. Windnagel., 2017 to present, updated daily: *Sea Ice Index, Version 3.*, doi:https://doi.org/10.7265/N5K072F8, Boulder, Colorado USA. NSIDC: National Snow and Ice Data Center. Accessed: April 1, 2019.

Graversen, R. G., T. Mauritsen, S. Drijfhout, M. Tjernström, and S. Mårtensson, 2011: Warm winds from the pacific caused extensive arctic sea-ice melt in summer 2007. *Climate dynamics*, **36 (11-12)**, 2103–2112.

Hakim, G. J., 2000: Climatology of coherent structures on the extratropical tropopause. *Monthly weather review*, **128 (2)**, 385–406.

Hanley, J., and R. Caballero, 2012: Objective identification and tracking of multicentre cyclones in the era-interim reanalysis dataset. *Quarterly Journal of the Royal Meteorological Society*, **138 (664)**, 612–625.

Hemer, M. A., J. Katzfey, and C. E. Trenham, 2013: Global dynamical projections of surface ocean wave climate for a future high greenhouse gas emission scenario. *Ocean Modelling*, **70**, 221–245.

Holt, B., and S. Martin, 2001: The effect of a storm on the 1992 summer sea ice cover of the beaufort, chukchi, and east siberian seas. *Journal of Geophysical Research: Oceans*, **106 (C1)**, 1017–1032.

Hoskins, B. J., M. McIntyre, and A. W. Robertson, 1985: On the use and significance of isentropic potential vorticity maps. *Quarterly Journal of the Royal Meteorological Society*, **111 (470)**, 877–946.

Inoue, J., and M. E. Hori, 2011: Arctic cyclogenesis at the marginal ice zone: A contributory mechanism for the temperature amplification? *Geophysical Research Letters*, **38 (12)**.

Intrieri, J., C. Fairall, M. Shupe, P. Persson, E. Andreas, P. Guest, and R. Moritz, 2002: An annual cycle of arctic surface cloud forcing at sheba. *Journal of Geophysical Research: Oceans*, **107 (C10)**.

Kay, J. E., T. L'Ecuyer, A. Gettelman, G. Stephens, and C. O'Dell, 2008: The contribution of cloud and radiation anomalies to the 2007 arctic sea ice extent minimum. *Geophysical Research Letters*, **35 (8)**.

Knudsen, E. M., Y. J. Orsolini, T. Furevik, and K. I. Hodges, 2015: Observed anomalous atmospheric patterns in summers of unusual arctic sea ice melt. *Journal of Geophysical Research: Atmospheres*, **120 (7)**, 2595–2611.

Kriegsmann, A., and B. Brümmer, 2014: Cyclone impact on sea ice in the central arctic ocean: a statistical study. *The Cryosphere*, **8 (1)**, 303.

Kwok, R., and G. Cunningham, 2010: Contribution of melt in the beaufort sea to the decline in arctic multiyear sea ice coverage: 1993–2009. *Geophysical Research Letters*, **37 (20)**.

Lammert, A., B. Brümmer, and L. Kaleschke, 2009: Observation of cyclone-induced inertial sea-ice oscillation in fram strait. *Geophysical Research Letters*, **36 (10)**.

Lind, S., R. B. Ingvaldsen, and T. Furevik, 2018: Arctic warming hotspot in the northern barents sea linked to declining sea-ice import. *Nature Climate Change*, **8 (7)**, 634.

Lovecraft, A. L., C. Meek, and H. Eicken, 2013: Connecting scientific observations to stakeholder needs in sea ice social–environmental systems: the institutional geography of northern alaska. *Polar Geography*, **36 (1-2)**, 105–125.

Markus, T., J. C. Stroeve, and J. Miller, 2009: Recent changes in arctic sea ice melt onset, freezeup, and melt season length. *Journal of Geophysical Research: Oceans*, **114 (C12)**.

Maslanik, J., J. Stroeve, C. Fowler, and W. Emery, 2011: Distribution and trends in arctic sea ice age through spring 2011. *Geophysical Research Letters*, **38 (13)**.

Mesquita, M. d. S., D. E. Atkinson, I. Simmonds, K. Keay, and J. Gottschalck, 2009: New perspectives on the synoptic development of the severe october 1992 nome storm. *Geophysical Research Letters*, **36 (13)**.

Mesquita, M. S., D. E. Atkinson, and K. I. Hodges, 2010: Characteristics and variability of storm tracks in the north pacific, bering sea, and alaska. *Journal of Climate*, **23 (2)**, 294–311.

Msadek, R., G. Vecchi, M. Winton, and R. Gudgel, 2014: Importance of initial conditions in seasonal predictions of arctic sea ice extent. *Geophysical Research Letters*, **41 (14)**, 5208–5215.

Murray, R. J., and I. Simmonds, 1991: A numerical scheme for tracking cyclone centres from digital data. *Australian Meteorological Magazine*, **39 (3)**, 155–166.

Neu, U., and Coauthors, 2013: Imilast: A community effort to intercompare extratropical cyclone detection and tracking algorithms. *Bulletin of the American Meteorological Society*, **94 (4)**, 529–547.

Nishii, K., H. Nakamura, and Y. J. Orsolini, 2015: Arctic summer storm track in cmip3/5 climate models. *Climate Dynamics*, **44 (5-6)**, 1311–1327.

Ogi, M., I. G. Rigor, M. G. McPhee, and J. M. Wallace, 2008: Summer retreat of arctic sea ice: Role of summer winds. *Geophysical Research Letters*, **35 (24)**.

Ogi, M., and J. M. Wallace, 2007: Summer minimum arctic sea ice extent and the associated summer atmospheric circulation. *Geophysical Research Letters*, **34 (12)**.

Ogi, M., K. Yamazaki, and J. M. Wallace, 2010: Influence of winter and summer surface wind anomalies on summer arctic sea ice extent. *Geophysical Research Letters*, **37 (7)**.

Overeem, I., R. S. Anderson, C. W. Wobus, G. D. Clow, F. E. Urban, and N. Matell, 2011: Sea ice loss enhances wave action at the arctic coast. *Geophysical Research Letters*, **38 (17)**.

Overland, J. E., and M. Wang, 2010: Large-scale atmospheric circulation changes are associated with the recent loss of arctic sea ice. *Tellus A: Dynamic Meteorology and Oceanography*, **62 (1)**, 1–9.

Parkinson, C. L., and J. C. Comiso, 2013: On the 2012 record low arctic sea ice cover: Combined impact of preconditioning and an august storm. *Geophysical Research Letters*, **40 (7)**, 1356–1361.

Perovich, D. K., J. A. Richter-Menge, K. F. Jones, and B. Light, 2008: Sunlight, water, and ice: Extreme arctic sea ice melt during the summer of 2007. *Geophysical Research Letters*, **35 (11)**.

Pierrehumbert, R., and K. Swanson, 1995: Baroclinic instability. *Annual review of fluid mechanics*, **27 (1)**, 419–467.

Reed, R. J., and B. A. Kunkel, 1960: The arctic circulation in summer. *Journal of Meteorology*, **17 (5)**, 489–506.

Rudeva, I., S. K. Gulev, I. Simmonds, and N. Tilinina, 2014: The sensitivity of characteristics of cyclone activity to identification procedures in tracking algorithms. *Tellus A: Dynamic Meteorology and Oceanography*, **66 (1)**, 24 961.

Schweiger, A., J. Zhang, R. Lindsay, and M. Steele, 2008: Did unusually sunny skies help drive the record sea ice minimum of 2007? *Geophysical Research Letters*, **35 (10)**.

Screen, J. A., I. Simmonds, and K. Keay, 2011: Dramatic interannual changes of perennial arctic sea ice linked to abnormal summer storm activity. *Journal of Geophysical Research: Atmospheres*, **116 (D15)**.

Sepp, M., and J. Jaagus, 2011: Changes in the activity and tracks of arctic cyclones. *Climatic Change*, **105 (3-4)**, 577–595.

Serreze, M., J. Box, R. Barry, and J. Walsh, 1993: Characteristics of arctic synoptic activity, 1952–1989. *Meteorology and Atmospheric Physics*, **51 (3-4)**, 147–164.

Serreze, M. C., 1995: Climatological aspects of cyclone development and decay in the arctic. *Atmosphere-Ocean*, **33 (1)**, 1–23, doi:10.1080/07055900.1995.9649522, URL https://doi.org/10.1080/07055900.1995.9649522.

Serreze, M. C., 2009: Northern hemisphere cyclone locations and characteristics from ncep/ncar reanalysis data, version 1.

Serreze, M. C., and A. P. Barrett, 2008: The summer cyclone maximum over the central arctic ocean. *Journal of Climate*, **21 (5)**, 1048–1065.

Serreze, M. C., F. Carse, R. G. Barry, and J. C. Rogers, 1997: Icelandic low cyclone activity: Climatological features, linkages with the nao, and relationships with recent changes in the northern hemisphere circulation. *Journal of Climate*, **10 (3)**, 453–464.

Serreze, M. C., A. H. Lynch, and M. P. Clark, 2001: The arctic frontal zone as seen in the ncep–ncar reanalysis. *Journal of Climate*, **14 (7)**, 1550–1567.

Shimada, K., T. Kamoshida, M. Itoh, S. Nishino, E. Carmack, F. McLaughlin, S. Zimmermann, and A. Proshutinsky, 2006: Pacific ocean inflow: Influence on catastrophic reduction of sea ice cover in the arctic ocean. *Geophysical Research Letters*, **33 (8)**.

Simmonds, I., C. Burke, and K. Keay, 2008: Arctic climate change as manifest in cyclone behavior. *Journal of Climate*, **21 (22)**, 5777–5796.

Simmonds, I., and K. Keay, 2009: Extraordinary september arctic sea ice reductions and their relationships with storm behavior over 1979–2008. *Geophysical Research Letters*, **36 (19)**.

Simmonds, I., and R. J. Murray, 1999: Southern extratropical cyclone behavior in ecmwf analyses during the frost special observing periods. *Weather and Forecasting*, **14 (6)**, 878–891.

Simmonds, I., R. J. Murray, and R. M. Leighton, 1999: A refinement of cyclone tracking methods with data from frost. *Aust. Meteor. Mag*, **28**, 617–622.

Simmonds, I., and I. Rudeva, 2012: The great arctic cyclone of august 2012. *Geophysical research letters*, **39 (23)**.

Solomon, S., D. Qin, M. Manning, K. Averyt, and M. Marquis, 2007: *Climate change 2007-the physical science basis: Working group I contribution to the fourth assessment report of the IPCC*, Vol. 4. Cambridge university press.

Squire, V., 2007: Of ocean waves and sea-ice revisited. *Cold Regions Science and Technology*, **49 (2)**, 110–133.

Steele, M., W. Ermold, and J. Zhang, 2008: Arctic ocean surface warming trends over the past 100 years. *Geophysical Research Letters*, **35 (2)**.

Stephenson, S. R., and L. C. Smith, 2015: Influence of climate model variability on projected arctic shipping futures. *Earth's Future*, **3 (11)**, 331–343.

Stephenson, S. R., L. C. Smith, L. W. Brigham, and J. A. Agnew, 2013: Projected 21st-century changes to arctic marine access. *Climatic Change*, **118 (3-4)**, 885–899.

Stroeve, J., E. Blanchard-Wrigglesworth, V. Guemas, S. Howell, F. Massonnet, and S. Tietsche, 2015: Improving predictions of arctic sea ice extent. *Earth and Space Science*, **96**, 11.

Stroeve, J., M. M. Holland, W. Meier, T. Scambos, and M. Serreze, 2007: Arctic sea ice decline: Faster than forecast. *Geophysical research letters*, **34 (9)**.

Stroeve, J. C., M. C. Serreze, M. M. Holland, J. E. Kay, J. Malanik, and A. P. Barrett, 2012: The arctic's rapidly shrinking sea ice cover: a research synthesis. *Climatic Change*, **110 (3-4)**, 1005–1027.

Tanaka, H., A. Yamagami, and S. Takahashi, 2012: The structure and behavior of the arctic cyclone in summer analyzed by the jra-25/jcdas data. *Polar Science*, **6 (1)**, 55–69.

Wadhams, P., 1981: The ice cover in the greenland and norwegian seas. *Reviews of geophysics*, **19 (3)**, 345–393.

Walker, G. T., 1923: Correlation in seasonal variation of weather. viii: A preliminary study of world weather. *Memoirs of India Meteorological Department*, **24**, 75–131.

Wang, M., and J. E. Overland, 2009: A sea ice free summer arctic within 30 years? *Geophysical research letters*, **36 (7)**.

Wei, L., T. Qin, P. Uotila, T. Vihma, B. Cheng, and Coauthors, 2016: Analyses of summer cyclone activities over the arctic ocean. *The 26th International Ocean and Polar Engineering Conference*, International Society of Offshore and Polar Engineers.

Woodgate, R. A., K. Aagaard, and T. J. Weingartner, 2006: Interannual changes in the bering strait fluxes of volume, heat and freshwater between 1991 and 2004. *Geophysical Research Letters*, **33 (15)**.

Woodgate, R. A., T. Weingartner, and R. Lindsay, 2010: The 2007 bering strait oceanic heat flux and anomalous arctic sea-ice retreat. *Geophysical Research Letters*, **37 (1)**.

Yamazaki, A., J. Inoue, K. Dethloff, M. Maturilli, and G. König-Langlo, 2015: Impact of radiosonde observations on forecasting summertime arctic cyclone formation. *Journal of Geophysical Research: Atmospheres*, **120 (8)**, 3249–3273.

Zhang, J., R. Lindsay, A. Schweiger, and M. Steele, 2013: The impact of an intense summer cyclone on 2012 arctic sea ice retreat. *Geophysical Research Letters*, **40 (4)**, 720–726.

Zhang, X., J. E. Walsh, J. Zhang, U. S. Bhatt, and M. Ikeda, 2004: Climatology and interannual variability of arctic cyclone activity: 1948–2002. *Journal of climate*, **17 (12)**, 2300–2317.

Zwally, H. J., J. C. Comiso, C. L. Parkinson, W. J. Campbell, and F. D. Carsey, 1983: Antarctic sea ice, 1973-1976: Satellite passive-microwave observations. Tech. rep., National Aeronautics and Space Administration Washington DC.